AN ABSTRACT OF THE THESIS OF

Josef G. Hortnagl for the degree of Master of Science in Mechanical Engineering presented on June 10, 2013

Title: Determination of Cohesive Parameters for Aerospace Adhesives

Abstract approved:

John P. Parmigiani

The use of adhesives in demanding engineering applications is a very common occurrence in the modern world. These adhesives are taking the role of many traditional fasteners, especially in the area of fiber reinforced composites. As the use of these adhesives become more common place, better understanding of their mechanics and failure methods are needed. Adhesives typically do not behave like metals under extreme loading, and so traditional failure analysis methods are not adequate. New numerical methods that combined strength and energy fracture mechanics have shown to be better modeling tools for adhesives. Cohesive zone analysis is one of those methods. This method is limited by the adhesive constitutive parameters that dictate how the cohesive elements will behave in the finite element analysis. There has been a number of studies focused on experimental methods for collecting these parameters, but there exist no prevalent database of values that can be used. The current study will use several different methods to collect cohesive parameters for a group of aerospace adhesives. This will allow researchers to more accurately model structures that use these adhesives, as well as understand strengths and weaknesses between the different testing methods. The adhesives tested in this study were Araldite AV4600, 3M DP420, Locktite E120, Hysol

E9359.3, and JB weld. A traction law device was used to investigate and calculate cohesive parameters in mode I and mode II loading. Additional test were used to collect individual cohesive parameters for the two loading modes. After testing was concluded traction laws were created and cohesive strength and toughness values generated. The different tests shows good agreement in most cases with some margin of error for different adhesives. The traction law device proved to be a capable tool for generating traction laws, but required special testing equipment and extensive post analysis. The process of collecting data with this device was time consuming and delicate. Due to these factors the results showed less agreement between test specimen groups and therefor carried less confidence in the parameters generated. The individual tests showed better agreement between test specimens and required less time for experiments and analysis. These however were not capable of generating full traction law curves.

Determination of Cohesive Parameters for Aerospace Adhesives

By

Josef G. Hortnagl

A THESIS

Submitted to

Oregon State University

in partial fulfillment of
the requirements for the
degree of

Master of Science

Presented June 10, 2013

Commencement June 2013

Master of Science thesis of Josef G. Hortnagl presented on

June 10, 2013.

APPROVED:

_____

Major Professor, representing Mechanical Engineering

_____

Head of the School of Mechanical, Industrial, and Manufacturing Engineering

_____

Dean of the Graduate School

I understand that my thesis will become part of the permanent collection of Oregon State University libraries. My signature below authorizes release of my thesis to any reader upon request.

_____

Josef G. Hortnagl, Author

ACKNOWLEDGEMENTS

I would like to thank my major professor and advisor Dr. John Parmigiani for his persistent help and confidence. He made it possible for me to be successful during my time as a graduate student and has presented me with numerous opportunities to gain knowledge and priceless experience. I would also like to show my appreciation for the other graduate students in Covell 240; Michael Summer, Brian Grimm, Andy Phan, Patrick Dailey, Bruce Bingham, Nasko Atanasof, Imran Hyder, and Andrew Otto. They have been a pleasure to work alongside and have always been there for help and support. Lastly I would like to acknowledge my parents Georg and Nancy Hortnagl for their support and confidence throughout my life.

TABLE OF CONTENTS

TABLE OF CONTENTS (Continued)

Page

TABLE OF CONTENTS (Continued)

Page

LIST OF FIGURES

LIST OF FIGURES (Continued)

Figure Page

LIST OF FIGURES (Continued)

Figure Page

LIST OF TABLES

Determination of Cohesive Parameters for Aerospace Adhesives

1. Introduction

1.1 Motivation

The use of adhesives in structural bonding is an increasingly common occurrence. The range of industries using adhesives is vast, as are the number of applications for adhesives. Adhesives have the ability to join surfaces of nearly any type of material as well as evenly distribute load throughout the joint. Adhesives also add far less weight than traditional fasteners [1]. More advanced adhesives are being developed for specific applications in structural components. The mechanical properties of these adhesives are rapidly increasing to meet new joint strength requirements. Better analysis methods are needed to properly study and design these adhesive joints [2]. Traditional methods do not accurately describe adhesives behavior when enduring stress. Traditional failure analysis methods in particular do not model the fracturing of adhesives correctly. Typically the analysis of fracture between joints was constrained to the use of either strength or energy based linear elastic fracture mechanics (LEFM). The strength based approach followed the work of Inglis [3] and relied on strength failure criteria that would depict crack propagation. This approach relies on determining critical stress concentration based on a critical crack tip radius to predict the onset of failure. His work would later lead to crack propagation prediction using stress intensity factors. The Griffith [4] type energy base failure criterion was created to address the infinite stress singularity that occurs at the crack tip using strength based LEFM [5]. This method is based on a thermodynamic analysis of the work required to create new crack surfaces. Irwin [6] later expanded on Griffith's method by defining a critical energy release rate that could be used to determine failure loading. However, in numerical studies LEFM can be susceptible to mesh dependence due to singularities that might occur [7]. The failure process zones in LEFM must be small in comparison with the near crack tip stress field.

This dictates that strength depends on the crack size and that a critical crack length will initiate a brittle fracture [8]. In materials that experience large scale bridging of large plastic deformations before crack propagation, LEFM can lead to inaccurate predictions. Other non-linear fracture mechanics models do not show significant improvement [9].

The inadequacies of LEFM are especially troublesome for industries that use composites and rely on adhesives to form strong and rugged joints. Without better analysis tools, such industries cannot have confidence in the life and performance of their designs [10]. Since the use of composite materials have continuously gained popularity and esteem in the engineering community, it is widely agreed that a better understanding of how to bond their structures with adhesive is required. The aerospace industry especially has taken advantage of reinforced polymer composites (RPCs) and structural adhesive joints. Revolutionary new aircraft designs, such as the Boeing 787 Dreamliner and Virgin Galactic, rely heavily on RPC and adhesive joints for approximately 50% of their primary structures [11] [12]. The automotive and sporting industries as well as the military are also using these more frequently [9]. Joining and bonding of RPC and other materials using adhesives is a field of study that has inspired many new ideas about fracture mechanics. These new methods attempt to address the insufficiencies in traditional LEFM analysis. One method that shows great improvement in analyzing adhesive joints is cohesive zone modeling. A consensus has been found in literature stating that for adhesives and large scale bridging analysis, cohesive zone models (CZM) are most appropriate [8] [13] [14] [15]Adhesive manufacturers have developed standardized material property testing procedures to help predict adhesive joint limitations. Typical industrial tests for determining adhesive properties are lap shear tests and lap peel tests. The lap shear test is used to determine the adhesive shear strength [16].These tests have some variations but most follow the same procedure. Samples are produced out of large sheet material substrates and bonded using an adhesive. After the adhesive

is cured, individual coupons are cut from the large panels. Each end of the coupon has an overlapping tab to allow the samples to be pulled in a shearing motion. The coupons are pulled in a tensile test and the peak shear strength recorded.

The lap peel test is used to measure the adhesive tensile strength [17]. Coupons are made out of individual strips of substrate and adhesive. These specimens are usually bonded in a double cantilever beam geometry with the free ends bent up at a right angle. This allows the coupons to be pulled in a peeling motion. The samples are then pulled apart in a tensile test and the peak peel strength is recorded. These values are used as reference values to help the designer choose appropriate adhesives based on their joint loading conditions. They do not allow the detailed analysis of how the adhesive could fail from a mechanics of materials approach and they do not directly relate to the properties of the adhesive. This not only severely limits their application for designing more demanding and complex structures but also limits the analysis of adhesive joint failure.

1.2 Background

The cohesive zone method is based on the work of Dugdale and later Barenblatt. Dugdale [18] superimposed stresses near the crack tip of small slits in steel sheets. He implied that plastic deformation occurs at the crack tip due to material yielding. He made the correlation between plastic zone length relationship and applied stress. Barenblatt [19] developed an equilibrium crack theory and proposed a process zone approach modeled after Dugdale's plastic zone. He used this relationship to create cohesion parameters for the crack front. These process zones were titled cohesive zones. The first recognized use of this method was by Hillerborg et al. [20] studying the damage behavior of concrete. Further work was done by Needleman [21] on micro damage in ductile materials and later Tvergaard and Hutchinson [22] on macroscopic crack extension in ductile materials [23]. Both used CZM-like methods for their analysis.

CZM is the main fracture determination method of the current work. This method relies on the combination of strength and energy based fracture mechanics. The cohesive zone itself is the fully formed process zone leading a crack tip. The length of the cohesive zone is a function of the material fracture length scale. For adhesives, this fracture length scale can be determined based on the dimensionless group: [15]

$$\frac{E\Gamma}{\sigma^2 l} \ll 1\ (for\ LEFM)\ or\ \frac{E\Gamma}{\sigma^2 l} > 1\ (for\ non\ LEFM)$$

where E is the substrate modulus, Γ is the adhesive cohesive toughness, σ is cohesive stress, l is the fracture length scale. The range of solutions for LEFM and non LEFM is determined based on the adhesive and substrate materials. It has been shown using FEA simulations that as this non-dimensional group becomes larger than one, error values between simulations and LEFM solutions drastically increase. [15]

The CZM can be visualized by a series of ligaments or elements acting in place of the adhesive. The ligaments span the adhesive thickness between the substrates. When loading is applied in either normal or shear directions the ligaments in cohesive zone deform. The ligaments near the crack tip begin deforming first. The deformation propagates until all the ligaments in the process zone have begun to deform. The fully formed process zone will continue to deform until a ligament reaches a critical crack opening displacement (δc).

At this point the ligament will fail and the crack tip propagates, as does the process zone. These steps are illustrated in Figure 1:

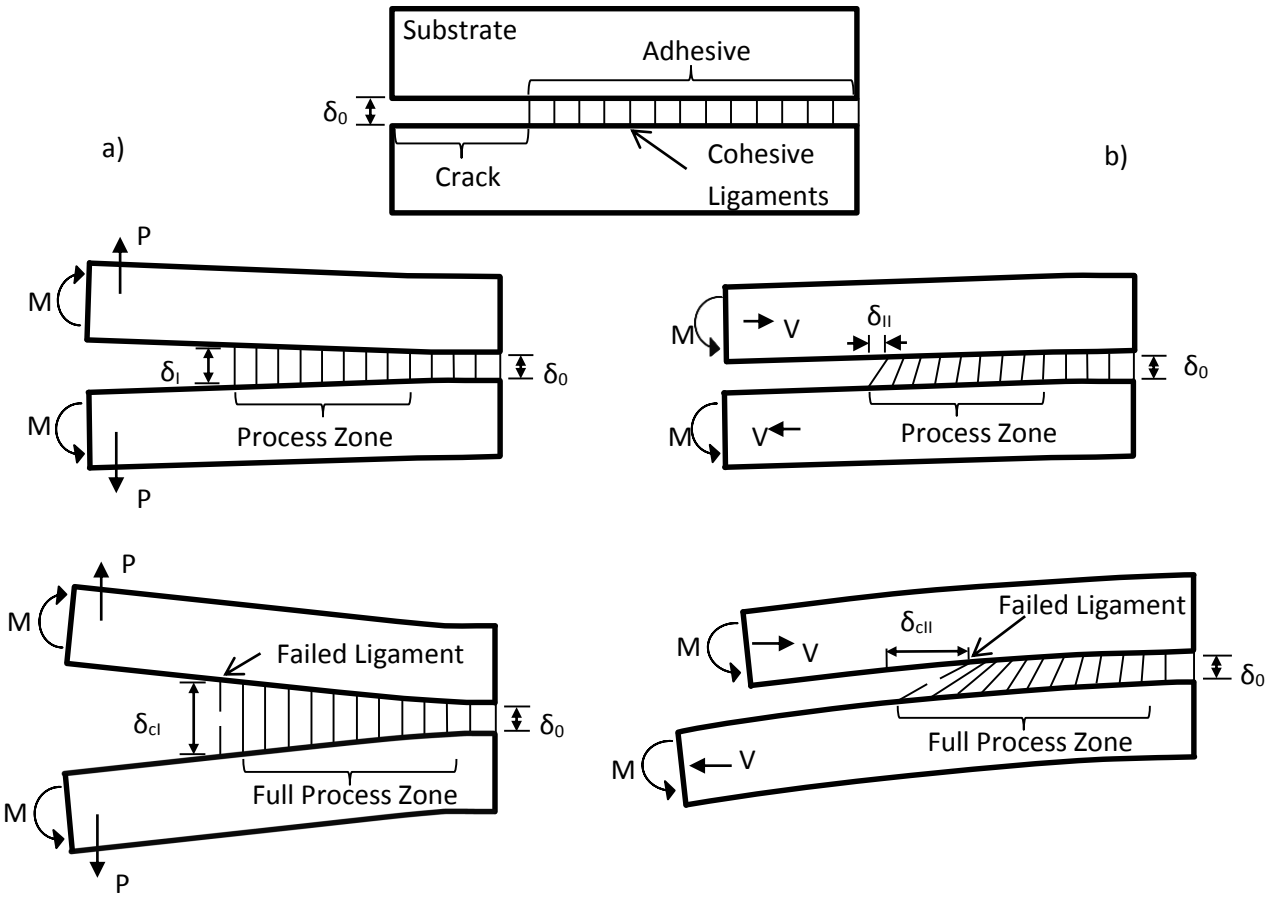

Figure 1: Deformation of Process zone for a) Mode I and b) Mode II

The behavior of these ligaments is based on the constitutive relation of the strength and energy based fracture methods. Typically a traction separation curve is used to dictate the ligaments behavior from the onset of loading to failure.

The CZM are typically associated with a traction-separation curve (TSC) depicting a materials' ability to carry load on a crack before it propagates. TLC are used when determining

cohesive parameters which will be denoted as the cohesive strength σ_c, the cohesive toughness Γ_c and critical crack opening displacement δ_c. Figure 2 illustrates the relationship between these parameters and their correlation with CZM:

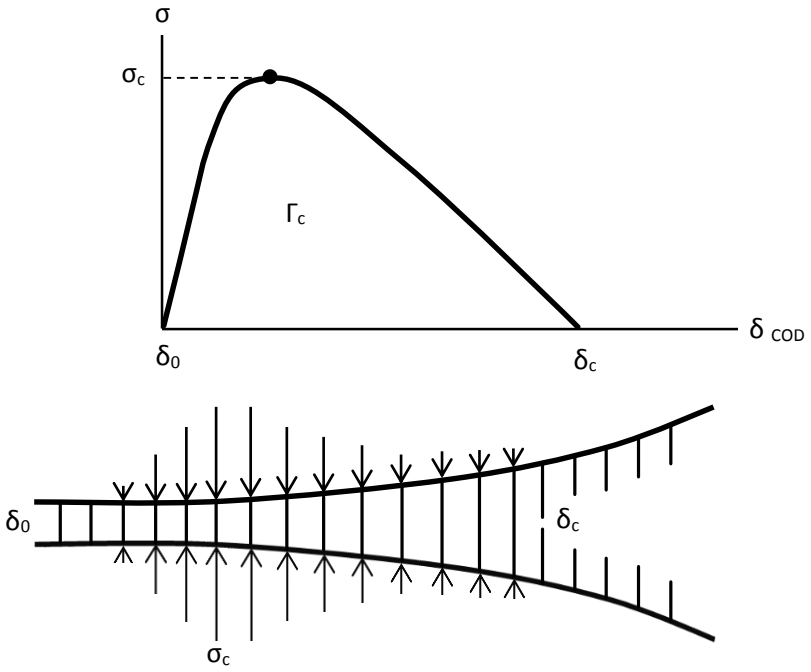

Figure 2: Constitutive relationship of cohesive values and associated joint deflection

Two independent values of these parameters will allow for the calculation of the third, assuming an ideal TSC. These parameters can be numerically estimated base off of fitting curves to TSC. Other general testing methods are suggested using tension specimens, but these have proven more useful as a starting point for the numerical fitting procedures [23]. The values for these TSC are also material and loading rate dependent [24]. So far TSC can be created for mode I, mode II, or mixed mode loading conditions. This study will focus on individual mode I and mode II TSC. Both mode I and mode II curves can be idealized as trapezoids.

Figure 3 illustrates the trapezoid model and the three main phases of a TSC.

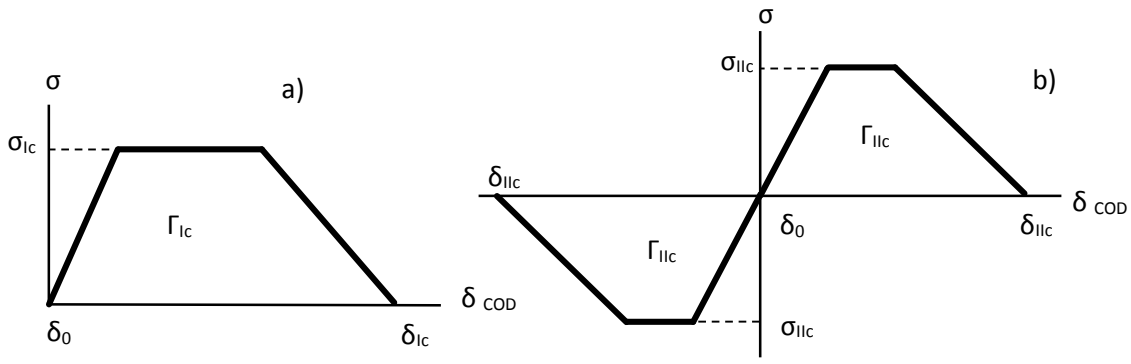

Figure 3: Trapezoid approximations of TSC for a) Mode I and b) Mode II

The first loading ramp often signifies the elastic proportion of loading on the adhesive. The next region signifies the plastic portion of loading on the adhesive. The critical separation energy approaches the interfaces' ability to carry load until it degrades to zero. At this point it is believed that a crack will grow as the interface can no longer support the load.

Often this ideal model is not true in shape to experimentally-generated curves but it has been determined that the curves' shape is somewhat superfluous. Depending on the interface material, different types of TSC can be generated. For instance, a brittle interface may have an extremely sharp, if not instantaneous, elastic and plastic section. This generally means that the interface can absorb little separation energy before fracture. This is commonly seen for brittle material. Oppositely a rather ductal interface may absorb the load and separation energy very gradually with a rapid damage and failure section. Regardless of the shape, the curve itself has three main characteristics that define it. The maximum stress peak determines the cohesive strength. The final opening displacement determines the critical crack opening displacement. The integrated area under the curve is known as the cohesive toughness. For adhesives, toughness is generally the most sought after property, mainly because it can be correlated using both FEA and LEFM

solutions. In many LEFM cases the critical surface energy characteristic, G, is synonymous with toughness. It is this relationship that allows the use of LEFM analytical solutions for some brittle adhesive joints. Creating these curves is not always a simple matter. In most cases determining the stresses across the adhesive limits experimental determination of TSC. The method used here employs the use of J-integral determination of the stresses across the adhesive.

The J-integral method was first introduced by Rice to extend fracture mechanics beyond the validity of LEFM [5]. This method is most appropriately used with materials with nonlinear deformation characteristics. This makes the J-integral method ideal for analyzing adhesives. Rice showed that a path independent contour integral around the crack tip, which he called J, could be equal to the energy release rate, G. The integral is considered path-independent because the integral of the stress tensor along a path is not affected by the path itself. This dictates that any complete path around the crack tip will give the same J value.

Sorenson proposed that using the J-integral to characterize the failure process zone was a possible way of determining bond line stresses [8]. Symmetric DCB specimens with pure bending moments applied to the ends were used to achieve this. He assumed that the failure process zones would be small compared to the characteristic length of the specimen beams. This allows the J-integral to evaluate traction along the external boundary of the specimen since the only non-zero contribution of the stress tensor is σ_{11}. Sorensen derived the following equation for evaluating J_{ext}:

$$J_{ext} = 12(1-\nu^2)\frac{M^2}{B^2H^2E}$$

where ν and E are the substrate Poisson's ratio and modulus respectfully, B and H are the specimen beam thickness and height, respectfully. Later, he extended this derivation to include

the possibility of mixed mode loading using uneven, and equal or opposing direction bending moments. [25] Following the same mechanical logic as before he derived the following mixed mode expression for J_{ext}:

$$J_{ext} = (1 - \nu^2)\frac{21(M_1^2 + M_2^2) - 6M_1M_2}{4B^2H^3E}$$

where ν and E are the substrate Poisson's ration and modulus respectfully, M_1 and M_2 are the two beam end moments, B and H are the specimen beam thickness and height, respectfully. For both of these derivations it is assumed that the substrates are the same material.

Sorenson then followed the approach first used by Li and Ward [26]to determine the bond line stresses. Since the J-integral calculates stress as a function of opening displacement using a path independent line integral, the stress can be determined by calculating the derivative of J with respect to opening displacement as follows:

$$\frac{\partial J}{\partial \delta} = \sigma(\delta)$$

Using this calculation it is possible to create a TSC by recording the beam end moments and the adhesive opening displacement during loading.

The developments in cohesive zone analysis that are most relevant to the current work come from the efforts of Thouless, Yang, Kafkalidis, and Sorenson. Thouless et al. [27] studied the toughness of plastically deforming joints. He used DCB specimens driven over a wedge to characterize cohesive parameters. Using three different adhesives he characterized toughness values based on glue-line thickness. He concluded that LEFM was not the correct method for analyzing these types of joints. Ferracin et al. [9] also used a wedge peel test as a method to determine cohesive zone properties. Yang [28] performed numerical analysis of adhesively bonded beams using cohesive zone method. Kafkalidis [29] performed similar studies of double

cantilever beam (DCB) specimens using the same adhesive as Yang. His resulting toughness and strength values correlated with Yang and Thouless's. All of these studies relied on analytical derivations from LEFM based fracture mechanics and embedded process zone analysis. As stated before sorenson [14] began a new series of studies involving adhesive joints. He began with studies on notch sensitivities of adhesive joints using cohesive laws. His approach used DCBs with end moments applied. The use of the path independent J-integral developed by Rice [30] allowed for the calculation of cohesive stresses. The loading fixture created by Sorenson [8] is similar to the fixture used in this study.

Many investigations focused on determining cohesive parameters for mixed mode loading. Choupani [31], Sorenson [25], Hogberg [32], and Moura [7] all investigated the effect mixed mode loading using cohesive modeling. Crack impingement which generally begins with the work of He and Hutchinson in the late eighties and nineties would later make use of cohesive elements. Parmigiani [15] studies the effects of cohesive parameters on crack deflection at interfaces. Parmigiani and Thouless [33] conducted a similar study on the effects of cohesive parameters on mixed mode loading of beam-like structures. Their approach relied on the use of FEA software with sub-routines for applying user defined cohesive elements properties.

Schwalbe et. al. [23] created a comprehensive method for applying cohesive elements using FEA. Amarasiri et al. (2011) experimentally back-calculated cohesive properties for clay material and geotechnical applications. Their approach tested side notch clay beams in three point bending. Samples were created at difference moisture contents. Mode I cohesive parameters were determined by recording load and load point displacement. These parameters were verified by using a distinct element program (UDEC). The study found agreement between the experimental and numerical applications for the cohesive parameters. Marzi et al. [24] [34] made efforts to extract adhesive mode II energy release rates with which they inferred cohesive values. They introduced unique testing geometries such as the tapered end-notched flexure (TENF) and the

end-loaded shear joint (ELSJ). Their efforts showed potential but were limited by the toughness of the applied adhesives.

1.3 Project Contribution

The study discussed here will directly determine cohesive parameters for specific adhesives intended for aerospace applications. Cohesive toughness and strength values for several adhesives will be collected using individual tests and a J-integral traction law test. Comparisons of testing methods used to collect cohesive values will be included. This is directly beneficial to researchers and industries using these adhesives and experimental methods. The cohesive parameter values can be used to accurately and efficiently model the behavior of these adhesives without the uncertainty or time consuming use of numerical determination methods. Also, the applicability and accuracy of the test methods used will provide further insight for future researchers. This will allow the determination of cohesive parameters for any type of structural adhesive in future studies.

2 Methods

2.1 Adhesives

The adhesives used in the study can be characterized as high strength. They were chosen from a number of sources that included industry recommendation and commercial product investigation. The four main adhesives used in this study were Araldite AV4600, 3M DP420, Locktite E120, Hysol E9359.3. An additional adhesive, JB Weld, was added to hopefully give the resulting group of parameters more range. JB Weld is a common craftsman adhesive that has gained favor with mechanics and technicians as a low cost high strength adhesive. The four main adhesives are advertised as high strength structural adhesive. AV4600 is the only thixotropic heat curing adhesive used in this study. The samples using AV4600 were cured in a heated shelf oven at 180 C for approximately 30 minutes. The samples were held in an aluminum heating pedestal to allow for even and quick temperature distribution along the glue line. Glue line temperatures were recorded using thermocouple wire for quality assurance. Thermocouple data was recorded using a National Instruments DAQ. All others adhesives were two parts chemically curing adhesive comprised of a resin base and a hardener. 3M DP420 and Locktite E120 came in container tubes designed to release the proper component ratio. Applicator guns were used to release the adhesive from the tubes. Hysol E9359.3 was mixed according to a weight ratio of 100:44 parts A to B. These separate components were dispensed into mixing cups and weighed to achieve the proper ratio. The two components were then combined and toughly mixed. JB Weld was mixed at a 1:1 ratio from small equal quantity foil tubes. To ensure proper mixing ratios, the entire tubes were used when mixing the adhesive components. Adhesive thickness was maintained by adding silica spheres to the adhesive in non-critical areas of the glue line. The silica beads created a uniform 0.6mm glue line that was determined as viable average of all the recommended glue line thicknesses. This adhesive thickness was used for all samples.

2.2 Transversely Loaded Double Cantilever Beams Test

Another method for measuring the mode I cohesive toughness for a specific adhesive is the transversely loaded DCB test. This method is based on an analytically derived solution from the work of Li et al [35].

Figure 4: Transversely Loaded Double Cantilever Beam Specimen Layout

This method is used to compare the values collected using the TLD. This will also serve as a comparable method for collecting cohesive toughness values for adhesives. An assumption is made to correlate the energy-release rate, G, to cohesive toughness, Γ. Based on this, the associated energy release rate for a symmetric DCB with joining layer (adhesive) can be expressed by:

$$G = \frac{12(Fa)^2}{\bar{E}h^3}\left(1 + 0.674\frac{h}{a}\right)^2$$

where F is transverse loading, a is crack length, $\bar{E}$ is the modified modulus given by $\bar{E}$=E/(1-v^2) where E and v are substrate modulus and Poisson ratio respectfully , and h is beam thickness.

DCBs identical to those used in the TLD are created, but are pulled apart transversely in a tensile tester. The recorded peak load is used to determine the associated cohesive toughness. Using identical adhesives, TLD and transversely load beam values can be compared.

2.3 Ligament Dogbone Tension Specimen Test

To compare the values of the cohesive strength calculated from the TLD, a ligament dogbone tensile (LDBT) test specimen geometry was used. This specimen utilized two bonded substrates with a simulated crack between two adhesive ligaments.

Figure 5: Ligament Dogbone Tension Specimen Layout

These ligaments are sized to allow for full process zone creation upon loading. This is calculated using the previously mentioned non-dimensional group $E\Gamma/\sigma^2 l=10$. This group is set to a value substantially greater than one on the assumption that the adhesive has substantial elastic and plastic deformation before failure. The samples are then pulled in tension until failure.

The associated peak stress calculated, according to failure load and ligament geometry, is the cohesive stress.

$$\sigma_I = \frac{P_{tension}}{A_{ligament}}$$

This method is limited in that an initial cohesive stress and toughness estimate are needed to determine the ligament geometry. Even though, this method can validate a preexisting cohesive stress value if the difference between the experimental results are low.

2.4 Ligament Shear Specimens Test

Similar to the LDBT Specimen, the ligament shear test specimen (LST) allows for the calculation of an adhesive cohesive strength in shear. This method relies on the same methodology for determine the specimen ligament length. The main difference between the LDBT and the LST is the method used to load the specimen. A specialized retrofit fixture was created for the TLD to allow these specimens to be loaded in pure shear. The retrofit constrains the specimen, allowing for only shear displacement. During the test a compressive force is applied to one end of the specimen, loading the adhesive line in shear.

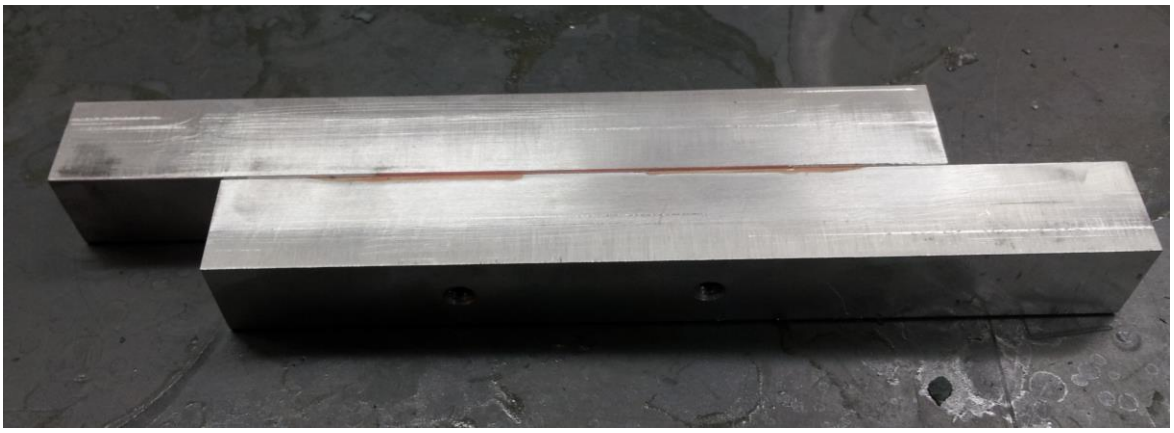

Figure 6: Ligament Shear Specimen Layout

The test is run until failure. The cohesive stress is calculated identically as the LDBT, using the applied compressive force and the ligament shear area:

$$\sigma_{II} = \frac{P_{compression}}{A_{ligament}}$$

This method also relies on an initial guess for mode II strength and toughness to determine the ligament length.

2.5 Shear Loaded Toughness Test

To measure mode II toughness a variant specimen was used from the works of Marzi et al. [24]. A long, thin substrate was used and analyzed similar to the TLB specimens, except in shear.

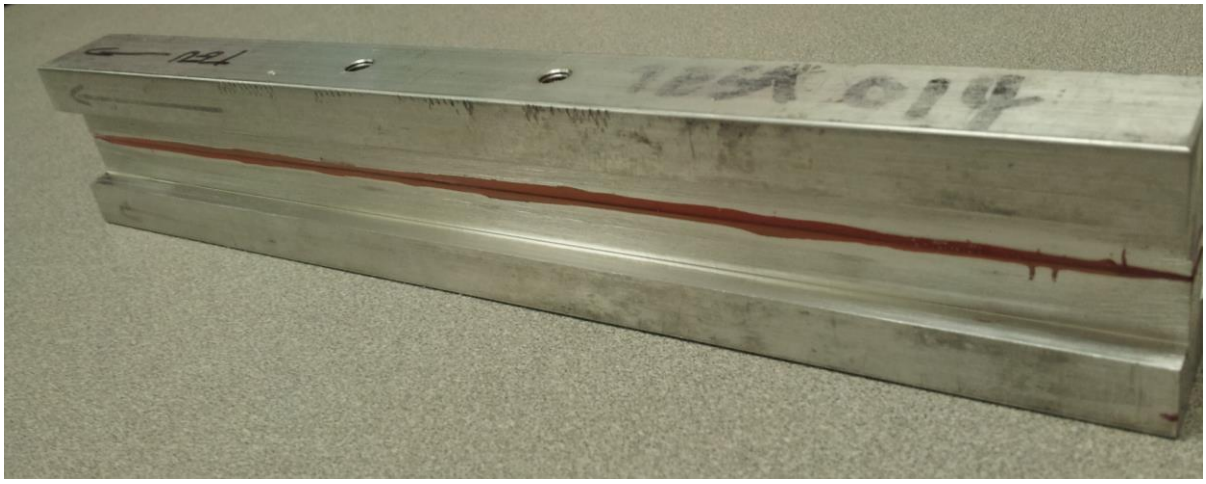

Figure 7: Shear Loaded Toughness Specimen Layout

The shear loading TLD retrofit was again used to apply a compressive load to one side of the specimen. A long ligament length was used to ensure that a fully formed process zone could be established. Modeled after the ELSJ specimen, the test samples substrates were long and thin. This allowed for a long shear ligament without requiring a failure force beyond the capacity of the tensile tester.

The analysis method for this specimen was considered with two levels of accuracy. Both consider the same assumption as the TLB, which correlates G to toughness. With these methods,

G is calculated using a stress intensity approach. From Tada's "The Stress Analysis of Cracks Book", *G* can be calculated using the following:

$$G = \frac{K^2}{E}$$

where K is the crack stress intensity factor and E is the bulk modulus. K is dependent on the loading and crack conditions and are determined by the specimen geometry used. A simplified scenario is defined by Tada as:

$$K_{II} = \frac{2}{\sqrt{\pi a}} Q F_{II}(a/b)$$

where a is the crack initiation length, Q is the shear force, and $F_{II}(a/b)$ is the correction factor for the specimen geometry, given by:

$$F_{II}(a/b) = \frac{1.30 - 0.65(a/b) + 0.37(a/b)^2 + 0.28(a/b)^3}{\sqrt{1 - a/b}}$$

where a/b is the ratio of crack initiation length to ligament length. This crack model could be considered vague because the associated loading geometry and loading scenario are only approximate. For a more applicable analysis method, the FEA program ABAQUS was used to determine the stress intensity factor. Modeling the specific geometry and loading scenario used, ABAQUS determined the crack tip stress intensity factor. Collapsed node quadrilateral elements were used around the crack tip and stress intensity values were created according to load applied.

2.6 Traction Law Device

The traction law device (TLD) is a custom loading fixture created based on the work of Sorenson. It is used to generate end moments on DCB specimens and was designed to be loaded into a tensile testing machine. End moments are generated using a cable and pulley system to create a couple on loading arms attached to the ends of the DCB. The entire device is comprised of two main fixtures; a lower and upper fixture. Figure 8 illustrates the layout of the TLD:

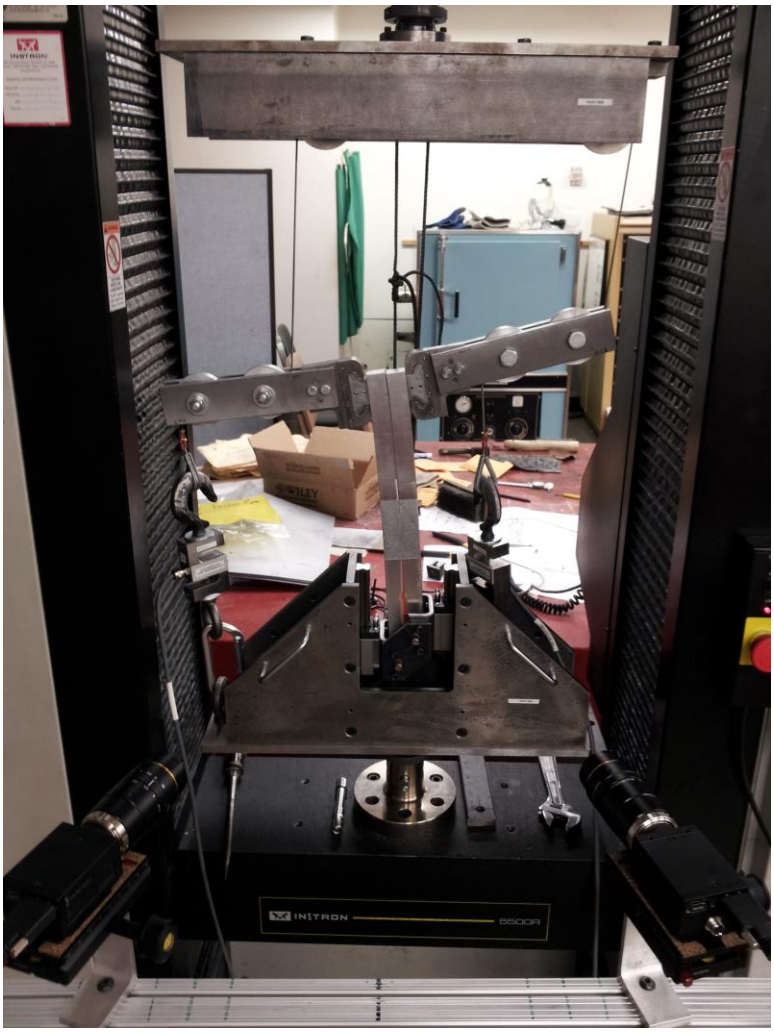

Figure 8: Traction Law Device loaded in the tensile tester

The lower fixture contains the attachment point for the base of the DCB specimens. Two offset pin connections on vertical linear sliders allow only one degree of freedom for the DCB specimen base. The lower fixture also contains the lower termination points for the moment arm

loading cable. This lower section fixes to the bottom restraint of the tensile tester. The upper fixture contains cable redirection pulleys. This fixture attaches to the top restraint of the tensile tester. As stated before, the applications of moments to the end of the DCB were achieved using two cable driven moment arms. The moment arms attach to the free ends of the DCB and contain two cable pulleys. A loading cable was routed from the lower fixture termination points, through the moment arms and upper redirection pulleys. In configuration 1, mode I loading can be achieved by creating equal and opposite couples in the moment arms. In configuration 2, mode II loading can be achieved by creating equal and same direction couples in the moment arms. A third configuration can be created for mixed mode loading by creating unequal and same direction couples in the moment arms. Loading is applied by separating the lower and upper fixtures which creates tensile forces in the cable and the associated moment arm couples. The tensile testing cross head speed was set at 1mm/min. Displacement ranges could be seen in literature from 0.3mm/min to 2mm/min [8] [14] [36] [37]. It was decided for quasi-static loading that 1mm/min was sufficient. Load cells were connected in line with the cables to measure the tensile force in each cable. This is used in the direct measurement of the moments generated by the moment arms. Along with recording the beam end moments, the specimen displacement was also needed. Sorensen used an extensometer attached to the specimen to accomplish this. For this study digital image correlation was used to gather sample crack displacement.

2.7 Digital Imaging Correlation

Digital Image Correlation (DIC) is an image based full field displacement measurement method pioneered by Ranson, Peters, Sutton, and Chao in the late 1980s. Later Sutton and McNeill would develop commercial analysis software VIC 3D. This software is used in the current study. DIC utilizes pixel intensities from digital images to calculate image displacement. For the purpose of simplification of pixel intensity quantification, gray scale images are used. Specimens are masked with a base color and fine speckle pattern of a contrasting color to create a dot matrix. The matrix can be applied using spray paint or air brushes, even colored powders can be applied for extremely fine speckles. For this study the area surrounding the end of the bond line was masked with white spray paint and speckled with black spray paint. Figure 9 shows a typical speckle pattern for the TLD samples:

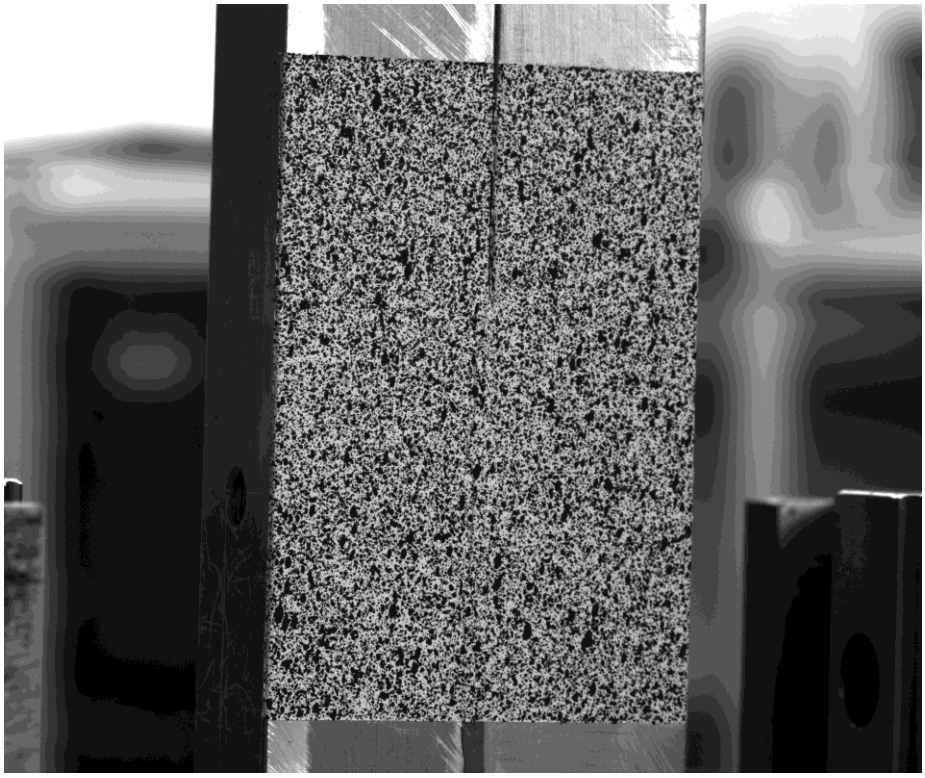

Figure 9: DIC speckle pattern for TLD samples

Images are taken in series and then incrementally compared to a reference image. Typically the reference image is at a state of non-loading. A region of interest (ROI) is selected and discretized into an N by N grid section. Pixel hue values are assigned to each pixel within the grid sections. From this, grid section centers (X_0,Y_0) are assigned [38] . The DIC algorithm searches for pixel intensity patterns from the reference image in the deformed image [39]. The associated deformed pixel pattern is assigned a new center (X_1,Y_1). Based on this comparison, displacement vectors C(Δu,Δv) of each grid section are determined.

This is typically done using a sum of squares difference function: [38]

$$C(\Delta u, \Delta v) = \sum_{n=-N}^{x=N} \sum_{y=-N}^{y=N} [f(x_0, y_0) - g(x_1, y_1)]^2$$

where F(x_0,y_0) is the reference image center pixel intensity, and g(x_1,y_1) is the deformed image center pixel intensity. This is continued over the entire ROI to create a displacement contour. Displacement accuracy is directly associated with grid spacing and size [39]. Coarse grid sizes will reduce overall field displacement accuracy, while being less computationally demanding. Oppositely, fine grid sizes will increase overall field displacement accuracy, but will be very computationally taxing.

This method was first developed for 2D analysis but was later extended to 3D applications. 3D DIC uses two simultaneously captured images at stereoscopic angles to each other. For this study two Point Gray Grasshopper 2 monochromatic cameras with lenses were used. A camera stage was constructed out of 80/20 extruded aluminum. The Cameras were set at 30 degrees angles towards the sample. Calibration is needed to define the analysis space used by the DIC algorithm. This is accomplished by capturing sequential images of a calibration grid at various angles and displacements in the analysis space. Based on the grid spacing on the calibration grid, the DIC software can calibrate spatial parameters such as size and depth. The calibration grid

used for this study was a 13 x 10 dot matrix with 3mm dot spacing. A minimum of 20 calibration images were captures and qualified before each test. The calibration also helps with other correction factors such as camera lens focal length, radial and tangential distortion, as well as image translation vectors and rotation matrices [40]. These are used to estimate a potential projection error for the analysis, as well as assist with image distortion.

2.8 TLD Sample Geometry

The samples run in the TLD were double cantilever beams bonded with adhesive. The beams were 375 mm long with a cross section 22.2mm by 22.2mm. The adhesive line was 170mm for mode I and 75 mm for mode II. The lengths of the bars was determined based off of Sorenson's test samples [25]. Additional length was also added to fit the tensile tester used.

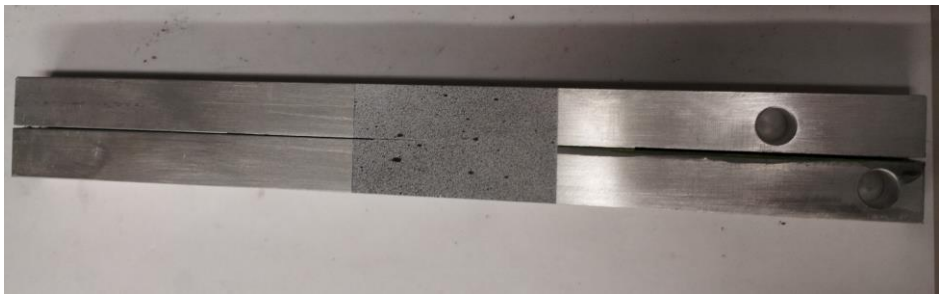

Figure 10: TLD test specimen with DIC speckle

The decision for a shorter adhesive line for mode II was made after difficulties fully fracturing samples with the original lengths was encountered. Full Sample dimensions are featured in appendix E. Threaded holes were machined into the free ends of the beams to allow a coupler to be attached using 5\16 cap screws. These couplers were the attachment points for the TLD moment arms. This is shown in Figure 11.

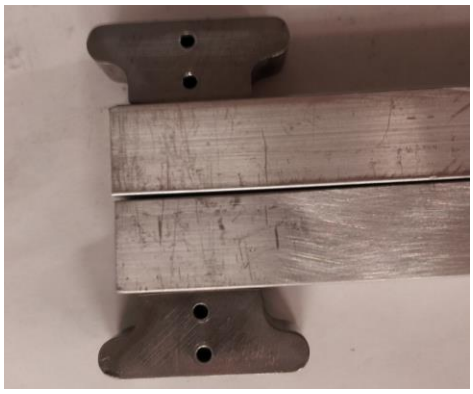

Figure 11: Moment arm couplers attached to the ends of the TLD sample

2.9 Sample Preparation

The most important aspect of the experimental work considered here was the creation of consistent cohesive crack initiations. Proper adhesion of the adhesive to the substrate was critical. There are a number of different factors that can effect adhesion such as substrate surface preparation, surface energy and wettability, surface contamination, and adhesive viscosity. The factors that received the most scrutiny were surface preparation and cleanliness. These were the factors that could be controlled the most strictly since the others mentioned are inherently material dependent.

Investigation into proper surface preparation and cleanliness revealed numerous different methods. The substrate material used was aluminum, which has specific requirements for bonding surfaces. Fresh aluminum will oxidize in the presence of oxygen. This is important because the aluminum oxide that naturally occurs can create a weak layer between the bulk material and the adhesive. To account for this, many methods suggest anodizing the aluminum surface to be bonded [41]. This was not possible for the current research due to time and cost constraints.

The use of surface primers was considered as an alternative to anodizing. In many industrial applications, a primer is used to create a better bonding surface for hard to adhere materials like plastics and some specialty metals. Primers generally consist of an extremely low viscosity adhesive agent that can better wet out (fully cover) the bonding surface. This is necessary if the

substrate material has low surface energy or slight contamination [1]. Primers create a thin layer of material that is designed to have optimal adhesion characteristics for the adhesive and substrate being used. Due to this specialized nature, many primers have an associated high cost and short shelf life. This would have required purchasing separate primers for all adhesives used, some of which did not have clear specifications. For these reasons, primers were not used in this study.

An alternate method recommended by adhesive manufactures suggested minimizing the amount of naturally forming aluminum oxide by abrading the surface. Since it was suggested that a comparable strength bond with the minimal external processing could be created, this was the chosen method for these experiments. The process consisted of several material removal steps using different abrasives. A final cross hatch pattern was abraded into the bonding surface just prior to adhesive application. This step would reveal fresh aluminum as well as give mechanical linkage points for the adhesive to flow into. To conserve the flatness of the substrates, the abrading steps were either performed against a straight belt sander, or with abrasive sheets attached to a flat work surface. When using abrasive sheets for the final cross hatch pattern, the samples were moved laterally in steady strokes at approximately 45. Initially 20 strokes to the right, then 20 strokes to the left, with 5 additional strokes to the right to bring out the crossed pattern. This is shown in Figure 12

Figure 12: Surface Preparation Using Abrasive Scoring

Between all preparation steps, the bonded surfaces were cleaned. Initially the substrates were washed with an industrial solvent after final manufacturing. Isopropanol alcohol was used between abrading steps and prior to bonding to remove any aluminum dust. Gloves were worn by the assemblers while handling the substrates to reduce the risk of contaminating the surface with natural oils. All abrasive sheets were vacuumed between samples to reduce the possibility of cross contaminating the substrates with aluminum dust.

2.10 Analysis

The product of the TLD tests are load cell data containing the cable tension and DIC displacement results. These data sets are analyzed using a program created in Matlab. The analysis program calculates the J-integral based on the load cell data. The COD data from the DIC analysis is then used with the J-integral calculations to determine the rate of change of j with respect to COD. Data smoothing techniques are used to reduce the effects of data noise on the

derivative calculation. This is then used to generate a TLC. From the TLC the different cohesive parameters can be determined. The TLC data outputs are imported to excel and further analyzed. The maximum point on the TLC is the cohesive strength. The end COD displacement where the strength returns to zero is the critical COD. Integrating the area under the TLC calculates the cohesive toughness value. After a sufficient number of curves have been generated, average cohesive parameters are calculated.

3 Results

3.1 Mode I Individual Test Results

3.1.1 Mode I Toughness

Figure 13 shows the resulting mode I cohesive toughness values generated from the transversely loaded beam specimens

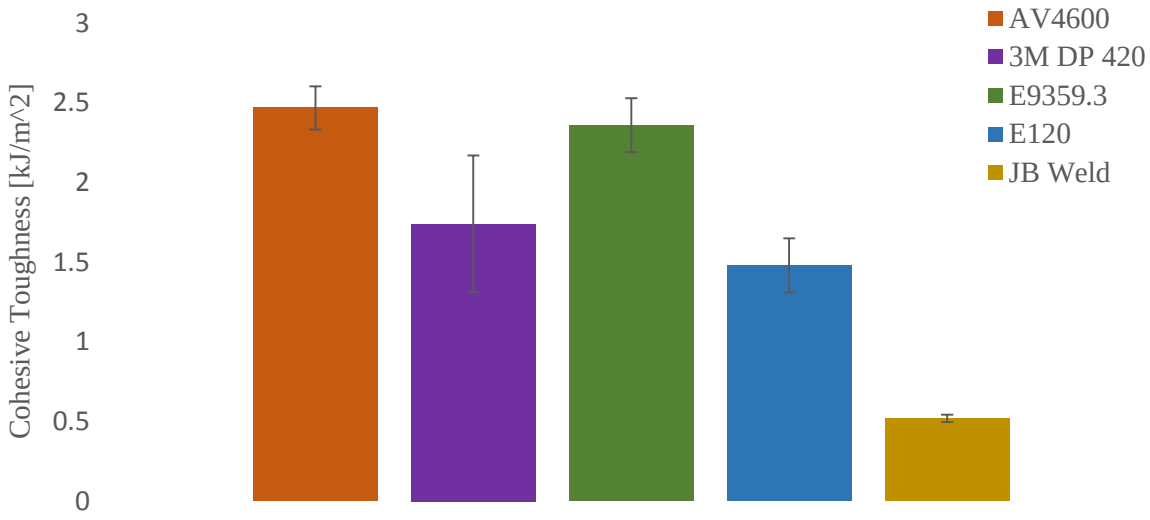

Figure 13: Transversely loaded beam specimen mode I cohesive toughness results. Error bars represent a 95% confidence interval.

3.1.2 Mode I Strength

Figure 14 shows the resulting mode I cohesive strength values generated from the dogbone ligament specimens

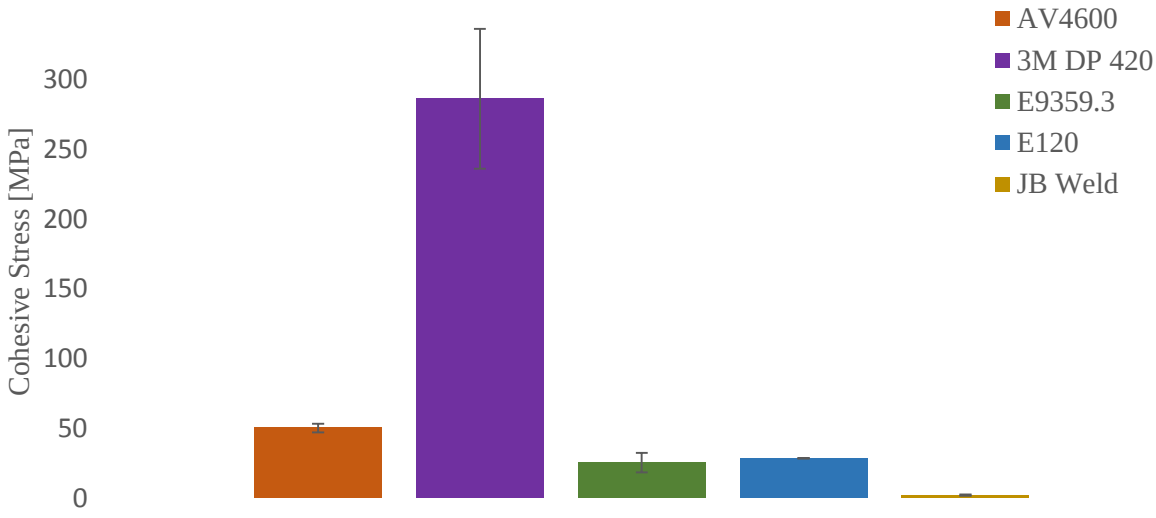

Figure 14: Dogbone ligament specimen mode I cohesive strength results. Error bars represent a 95% confidence interval.

3.2 Mode II Individual Test Results

3.2.1 Mode II toughness

Figure 15 shows the resulting mode I cohesive strength values generated from the shear toughness test specimens

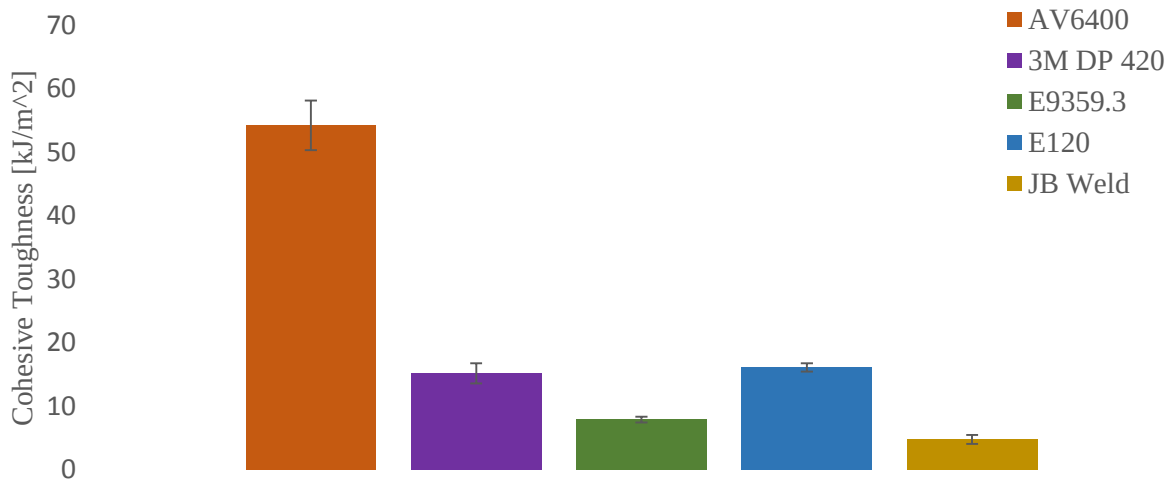

Figure 15: Shear toughness test specimen mode II cohesive toughness results. Error bars represent a 95% confidence interval

3.2.2 Mode II Strength

Figure 16 shows the resulting mode II cohesive strength values generated from the shear ligament test specimens

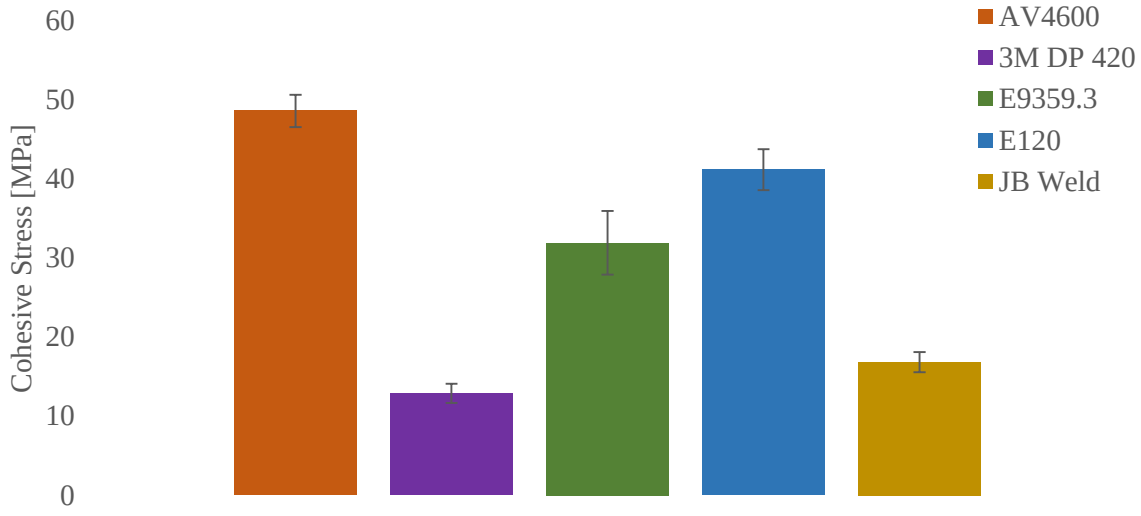

Figure 16: Shear ligament test specimen mode II cohesive strengths results. Error bars represent a 95% confidence interval

3.3 Mode I TLD Results

3.3.1 AV4600

Figure 17 shows the average TLC generated for AV4600 for Mode I.

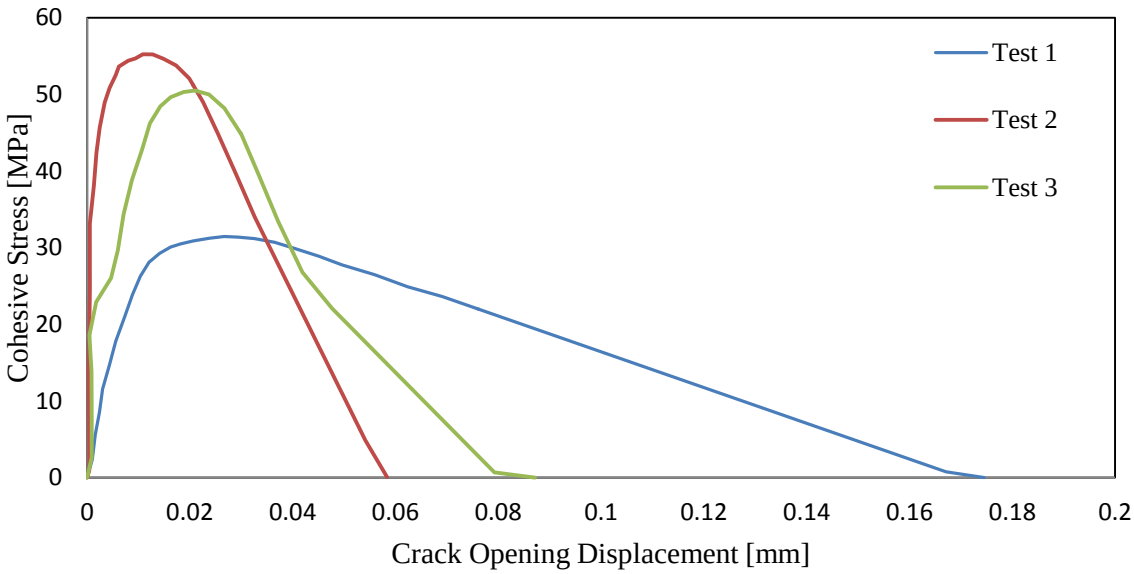

Figure 17: TLC for AV4600 for Mode I tests..

3.3.2 3M DP 420

Figure 1 shows the average TLC generated for 3M DP 420 for Mode I.

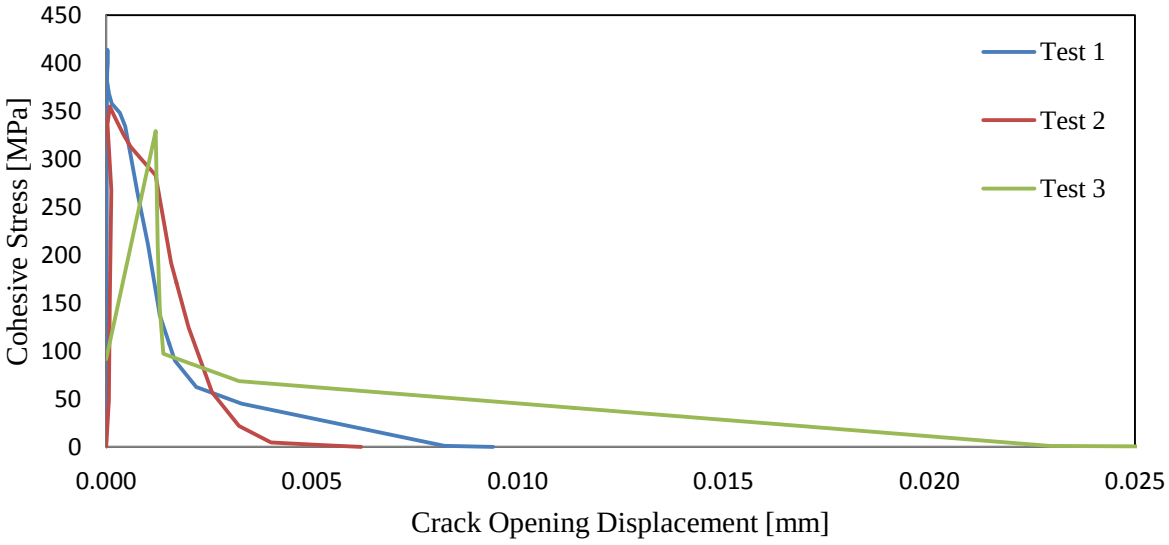

Figure 18: TLC for 3M DP 420 for Mode I tests.

3.3.3 Locktite E120

Figure 19 shows the average TLC generated for Locktite E120 for Mode I.

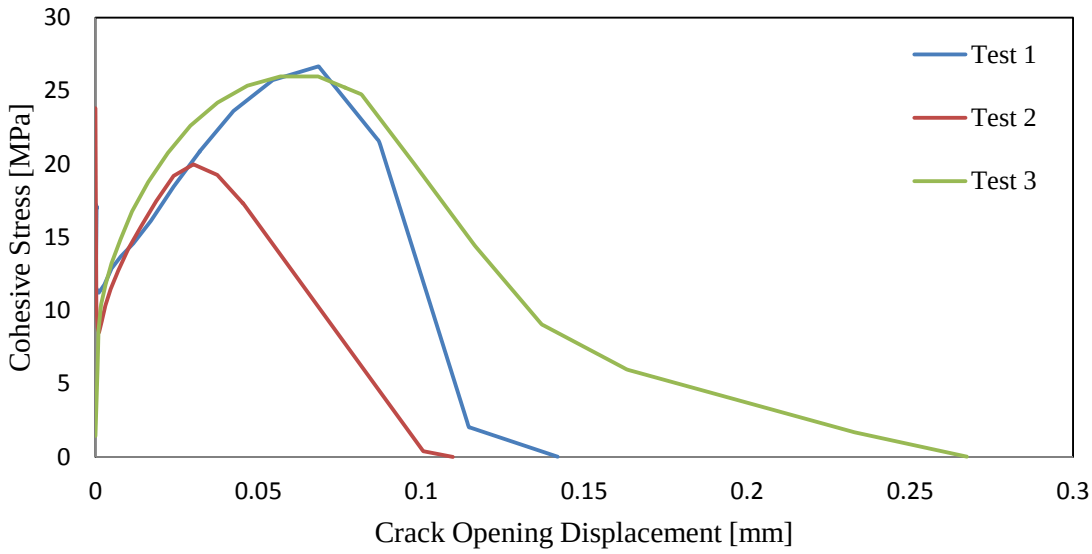

Figure 19: TLC for Locktite E120 for Mode I tests..

3.3.4 Hysol E9359.3

Figure 20 shows the average TLC generated for Hysol E9359.3 for Mode I.

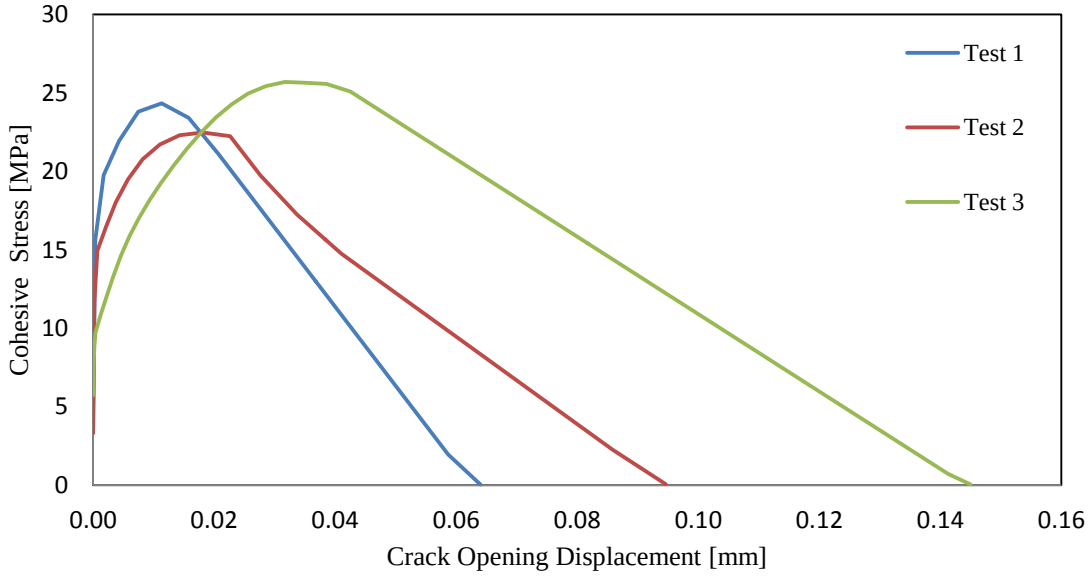

Figure 20: TLC for Hysol E9359.3 for Mode I tests.

3.3.5 JB Weld

Figure 21 shows the average TLC generated for JB Weld for Mode I.

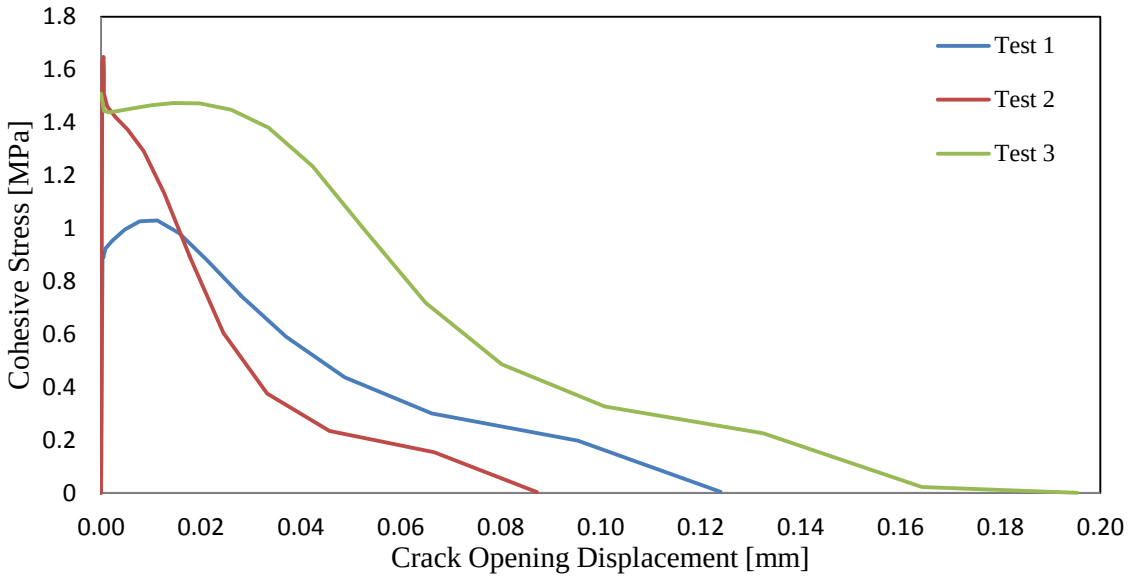

Figure 21: TLC for JB Weld for Mode I tests.

3.4 Mode II TLD Results

3.4.1 AV4600

Figure 22 shows the average TLC generated for AV4600 for Mode II.

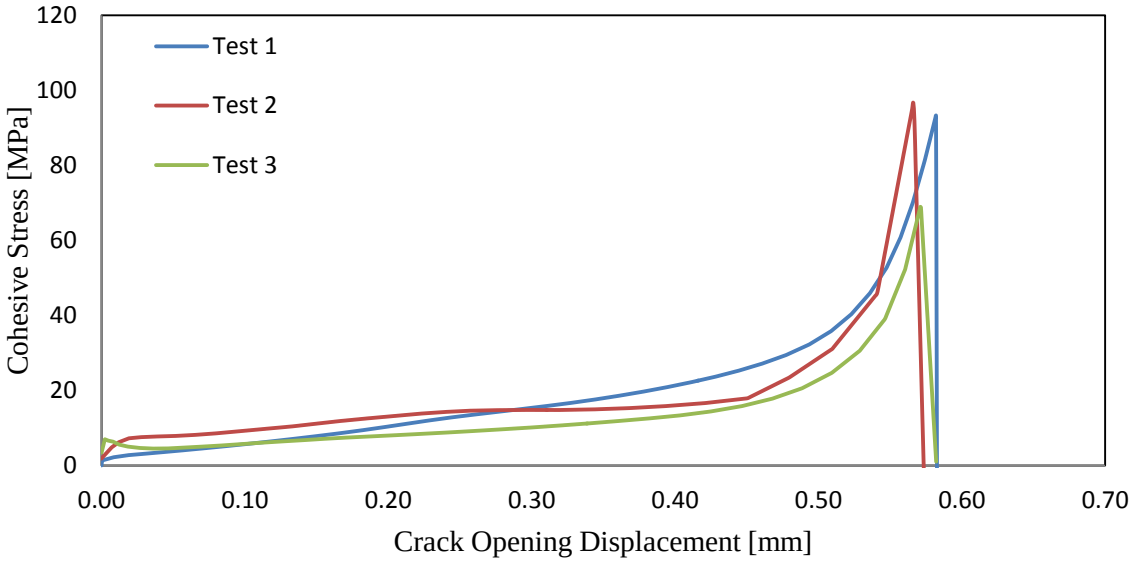

Figure 22: TLC for AV4600 for Mode II tests.

3.4.2 3M DP 420

Figure 23 shows the average TLC generated for 3M DP 420 for Mode II.

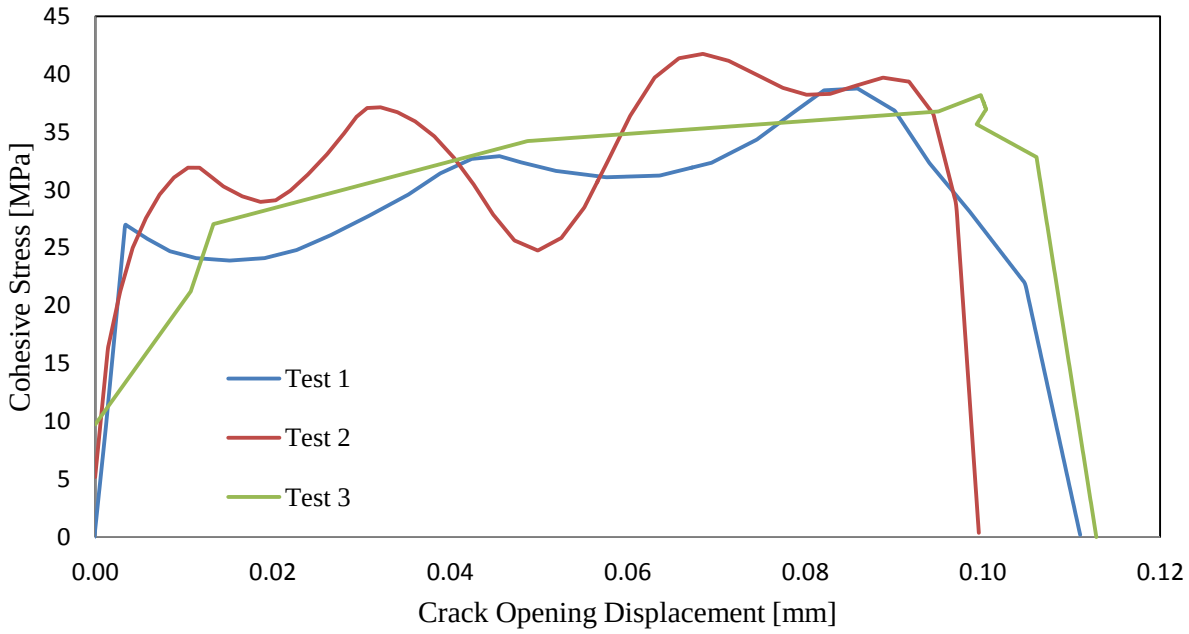

Figure 23: TLC for 3M DP 420 for Mode II tests.

3.4.3 Locktite E120

Figure 24 shows the average TLC generated for Locktite E120 for Mode II.

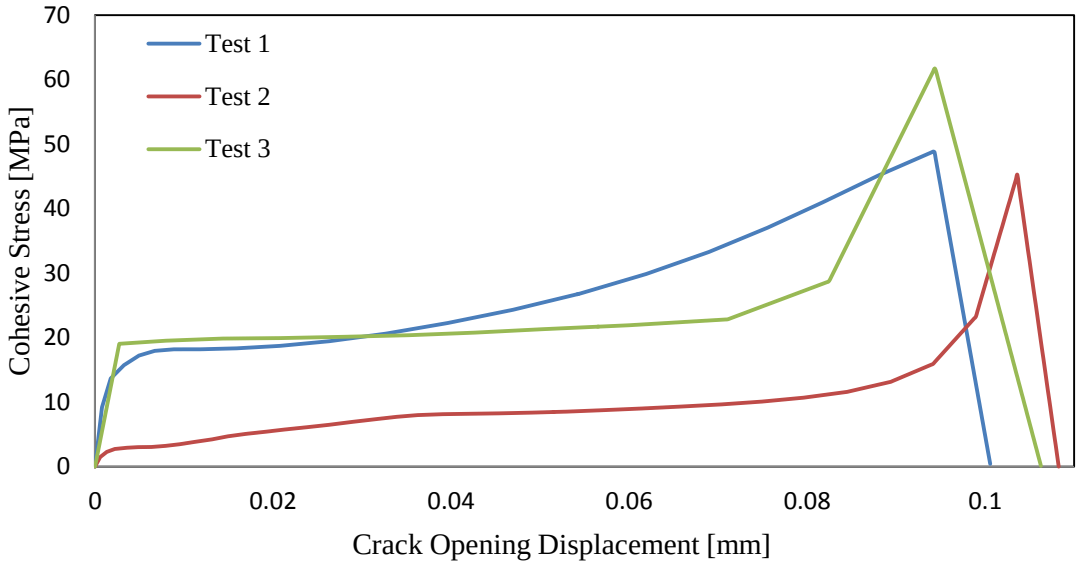

Figure 24: TLC for Locktite E120 for Mode II tests.

3.4.4 Hysol E9359.3

Figure 25 shows the average TLC generated for Hysol E9359.3 for Mode II.

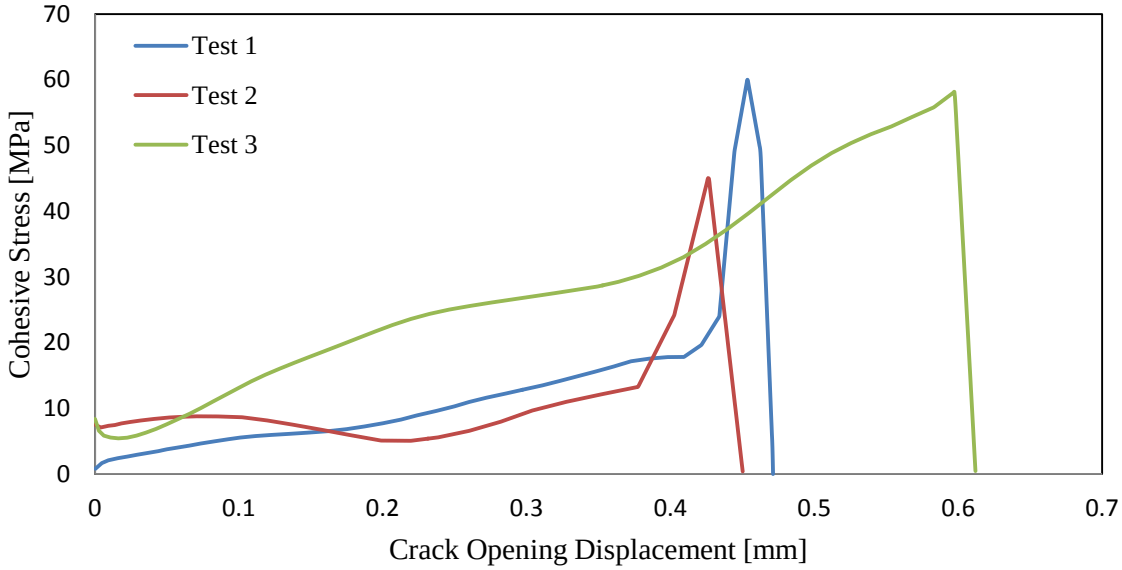

Figure 25: TLC for Hysol E9359.3 for Mode II tests.

3.4.5 JB Weld

Figure 26 shows the average TLC generated for JB Weld for Mode II.

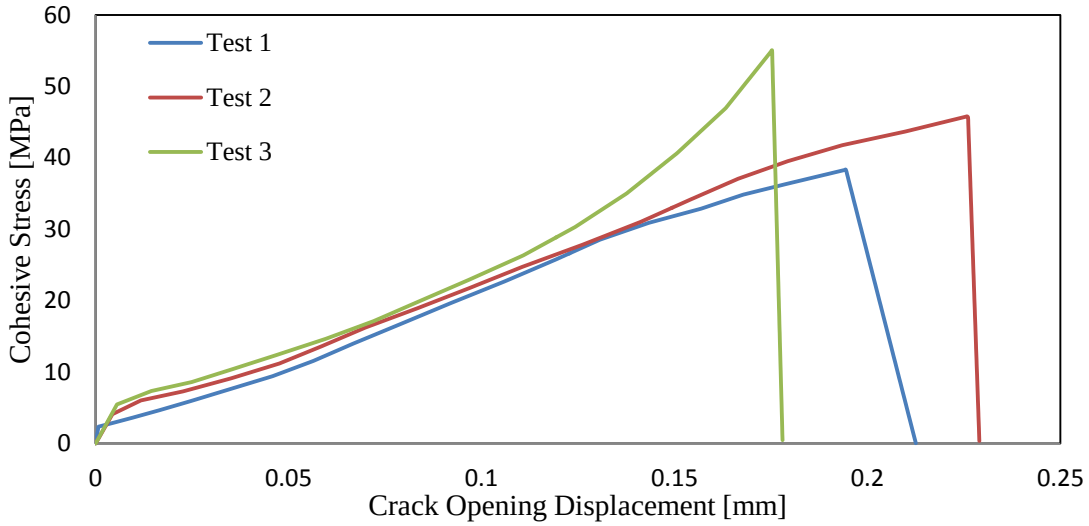

Figure 26: TLC for JB Weld for Mode II tests.

3.5 Transversely Loaded Double Cantilever Beam Results

3.5.1 Test Results

The following table includes results from the test completed to summarize mode I cohesive toughness

Table 1: Transversely loaded double cantilever beam summary

	Mode I Cohesive Toughness [kJ/m^2]				
	AV4600	3M DP 420	E9359.3	E120	JB Weld
Test 1	2.35	1.99	2.39	1.33	0.53
Test 2	2.59	1.31	2.50	1.62	0.52
Test 3	2.48	1.93	2.20	1.49	0.49
Average	**2.47**	**1.74**	**2.36**	**1.48**	**0.52**
STDEV	**0.12**	**0.38**	**0.15**	**0.15**	**0.02**

3.6 Ligament Dogbone Tension Specimen Results

3.6.1 Test Results

The following table includes results from the test completed to summarize mode I cohesive Stress

Table 2: Ligament dogbone tension specimen summary

	Mode I Cohesive Stress [MPa]				
	AV4600	3M DP 420	E9359.3	E120	JB Weld
Test 1	53.36	297.97	23.21	28.59	2.29
Test 2	48.65	323.41	32.36	28.16	1.62
Test 3	48.58	237.21	20.61	28.49	2.44
Average	**50.20**	**286.19**	**25.40**	**28.41**	**2.12**
STDEV	**2.74**	**44.29**	**6.17**	**0.22**	**0.44**

3.7 Shear Loaded Toughness Specimen Results

3.7.1 Test Results

The following table includes results from the test completed to summarize mode II cohesive toughness. Both the Handbook and the FEA approximations are included

Table 3: Shear loaded toughness specimen summary

	Mode II Cohesive Toughness [kJ/m^2]									
	AV4600		3M DP 420		E9359.3		E120		JB Weld	
	FEA	Book	FEA	Book	FEA	Book	FEA	Book	FEA	Book
Test 1	50.49	55.19	16.30	17.81	7.80	8.52	16.64	18.18	4.64	5.07
Test 2	57.27	62.60	15.63	17.08	7.56	8.26	15.51	16.94	5.44	5.94
Test 3	54.97	60.09	13.59	14.85	8.31	9.08	16.18	17.68	4.22	4.62
Average	**54.24**	**59.29**	**15.17**	**16.58**	**7.89**	**8.62**	**16.11**	**16.62**	**4.77**	**5.21**
STDEV	**3.45**	**3.77**	**1.41**	**1.54**	**0.39**	**0.42**	**0.57**	**1.38**	**0.62**	**0.67**

3.8 Ligament Shear Specimen Results

3.8.1 Test Results

The following table includes results from the test completed to summarize mode II cohesive stress

Table 4: Ligament shear specimen summary

	Mode II Cohesive Stress [MPa]				
	AV4600	3M DP 420	E9359.3	E120	JB Weld
Test 1	46.80	12.21	27.82	38.77	18.12
Test 2	50.43	12.28	34.34	41.37	16.24
Test 3	48.56	14.12	33.54	43.33	16.09
Average	**48.60**	**12.87**	**31.90**	**41.15**	**16.82**
STDEV	**1.82**	**1.08**	**3.56**	**2.29**	**1.13**

3.9 TLD Values

3.9.1 Mode I TLD Toughness Values

The following table includes resulting toughness for the Mode I TLD tests.

Table 5: Mode I TLD values for toughness

	Mode I Cohesive Toughness [kJ/m^2]				
	AV4600	3M DP 420	E9359.3	E120	JB Weld
Test 1	3.04	0.61	0.90	2.08	0.55
Test 2	1.99	0.60	1.19	1.79	0.41
Test 3	2.17	1.12	2.20	3.08	1.13
Average	**2.40**	**0.78**	**1.43**	**2.32**	**0.69**
STDEV	**0.56**	**0.30**	**0.68**	**0.68**	**0.38**

3.9.2 Mode I TLD Strength Values

The following table includes resulting strength for the Mode I TLD tests.

Table 6: Mode I TLD values for strength

	Mode I Cohesive Strength [MPa]				
	AV4600	3M DP 420	E9359.3	E120	JB Weld
Test 1	31.47	413.44	24.34	25.39	1.03
Test 2	55.24	354.67	22.48	25.39	1.65
Test 3	50.51	329.17	25.70	24.74	1.51
Average	**45.74**	**365.76**	**24.17**	**25.17**	**1.40**
STDEV	**12.59**	**43.22**	**1.62**	**0.37**	**0.32**

3.9.3 Mode II TLD Toughness Values

The following table includes resulting toughness for the Mode II TLD tests.

Table 7: Mode II TLD values for toughness

	Mode II Cohesive Toughness [kJ/m^2]				
	AV4600	3M DP 420	E9359.3	E120	JB Weld
Test 1	7.55	3.19	5.87	2.72	4.36
Test 2	8.11	3.28	4.91	1.12	5.76
Test 3	7.99	3.46	17.46	2.64	4.15
Average	**7.89**	**3.31**	**9.41**	**2.16**	**4.75**
STDEV	**0.29**	**0.14**	**6.99**	**0.91**	**0.87**

3.9.4 Mode II TLD Strength Values

The following table includes resulting strength for the Mode II TLD tests.

Table 1: Mode II TLD values for strength

	Mode II Cohesive Strength [MPa]				
	AV4600	3M DP 420	E9359.3	E120	JB Weld
Test 1	93.31	38.76	60.00	48.85	38.34
Test 2	96.64	41.75	45.03	45.26	45.81
Test 3	68.95	38.19	58.15	61.74	55.08
Average	**86.30**	**39.57**	**54.39**	**51.95**	**46.41**
STDEV	**15.12**	**1.91**	**8.16**	**8.67**	**8.38**

4 Discussion

4.1 Individual Cohesive Parameter Tests

The individual tests used for gathering strength and toughness values proved to be simple to run and gave consistent results. The individual tests required some specialized equipment but in general were much simpler to run than the TLD. Mode I strength and toughness tests only required the use of a pin coupler to attach the sample to the tensile tester. The consistency between these tests was very good and repeatable. Consistent cohesive fracture was also seen for these tests. The post processing was minimal which greatly reduced the risk of possible data distortion. Mode II toughness and strength tests required a retrofit of the lower fixture on the TLD to hold the sample during the test. Again these tests were simple and showed consistent results. The analysis for these samples was also uncomplicated. Good agreement was found between the hand book stress intensity approach and the FEA analysis for mode II toughness calculations. The hand book solution for the sample geometry gave higher toughness values than those provided by FEA analysis. This is most likely because the FEA model more accurately reflects the test sample geometry than the values presented by the hand book solution. As a result, the FEA values for toughness were chosen to represent the cohesive parameters. The drawback of these simple tests are that only the cohesive values are generated and TLCs still need to be approximated using idealized shapes. This makes the determination of the critical crack opening displacement dependent on the type of curve approximation used. A high degree of confidence was given to these test results mainly due to their simple nature and the good agreement between tests. It is the author's opinion that these test results reflect the true cohesive parameters of the adhesives.

4.2 TLD Results

The TLD designed and used in this study was able to successfully generate TLCs. The need for such a complicated piece of equipment to generate TLCs is a major short coming of this method. The investment put into this device was intended to allow for easy determination of entire TLCs, something that has proven to be difficult in the literature. While this device was

functionally modeled after that of Sorensen, the overall design was tailored to work with the equipment at hand. Some design revisions became apparent during the device's use, and as a result, the final design of the TLD is unique.

There are several positive and negative aspects to the current TLD. The device was well constructed and rugged enough for testing the samples used. The overall maintenance of the device was limited to proper storage and set up. Some slight wearing of the cable pulleys was noticed, but this did not result in any noticeable effect on performance. The modular attachment points for the cable terminations, load cell attachment points, and pulleys allowed for relatively easy reconfiguration from mode I to II and vice versa. Loading samples in and out of the lower fixture was rather challenging, since the pins restraining the samples were often difficult to align. This was mainly due to the restricted space between the sliders and the TLD support structure. The difference between the tensions in the cables increased dramatically (>20lbs) after loads over 600 lbs. This was more apparent in mode II than in mode I. The tension difference could be due to a lack of rotation of the pulleys to equalize the tensile load. Different bearing types such as roller bearings could better handle the transvers loading. Overall, the device was moderately easy to use once the user understood its operating procedures. An untrained operator would find the device rather complicated to operate.

The samples run in the device generally offered decent results with some abnormalities. It can be stated plainly that samples run in mode I often ran more consistently than in mode II, with clear crack initiation and full fracture of the sample. The mode II samples seemed more reluctant to fracture. This could be interpreted as a tendency of the adhesive to hold more stress in mode II. The reluctance to fracture could also illustrate the higher cohesive stresses seen from the mode II TLD results.

The data collected from the load cells and DIC analysis proved to be robust with little noise. The quasi steady state loading rate gave smooth cable tension readings as well as crack opening displacements. The data did require several smoothing steps while calculating the J-integral and the derivative of the J-integral with respect to crack opening displacement. Without these steps, even slight noise in the data could render the end traction law incomprehensible. Great care and scrutiny was taken in sample preparation, and all samples within a set were produced at the same time under the same conditions using the same adhesive. Samples were also not allowed to age for more than 10 days, as any time effects on the adhesive were not desired. Again all samples were cleaned and prepped for DIC speckle in the same manner as curing. The method for applying the DIC speckle was perhaps the most unregulated, as different spray can produce different speckle intensity and size. This however is not a very likely candidate for sample inconsistency, since every speckle pattern was checked beforehand for accuracy in displacement and strain calculation. Adhesive thickness levels were also monitored by measuring each substrate and cured sample. Noticeable deviation from the desired thickness was never encountered, so it is not likely that this had any effect on the sample analysis success rate. Efforts were made to quantify the modulus of the substrate beams being used. These efforts to accurately measure modulus values for each substrate proved unsuccessful. The use of a sonographic modulus detector was attempted, but difficulties with the required sample geometry greatly reduce the confidence in these results. Assumed modulus values were used from manufacturing specification. This assumption is not likely to have significant effect on the adhesive performance.

4.3 Test Comparison

A key investigation of this study was the degree of agreement between individual tests and TLD results. If the TLD method was sound, there should be good agreement between the different cohesive values. This study shows some agreement as well as disagreement between the different tests. For mode I most of the adhesives studied showed similar results between the

individual test and TLCs. AV4600 showed the best agreement of all the adhesives at 11% and 8% differences in its toughness and strength values, respectfully. The other adhesives showed moderate agreement between values, showing approximately 20% to 40% agreement. Little agreement was shown between tests from mode II. TLD test results for both toughness and strength were much lower. The mode II cohesive strength values for AV4600 was the only TLD value greater than those of the simple tests. Only JB weld showed good agreement between toughness values at 0.2% difference. The only other agreement was for the cohesive strength of E120, showing a 20% difference.

The results of the current tests correlated well with values found in literature. Values collected for different adhesive by Kafkalidis et al. had variations on the order of ± 15 to 20 MPa for cohesive stress and ± 0.2 kJ/m^2 for cohesive toughness [42]. For most of the adhesive used in this study, cohesive strength values fell within this same range, and in some cases showed improvement. For example AV4600 run in the TLD in mode I had a deviation of ±12.6 MPa for cohesive strength. The individual tests for both mode I and mode II showed better correlations between tests than literature. The majority of these test had standard deviations from 0.22 MPa to 6.17 MPa, with DP 420 having the highest standard deviation at 44.29 MPa. Toughness values did have slightly higher deviations than literature. Most adhesive run in the TLD showing ranges from ± 0.3 kJ/m^2 to ±1 kJ/m^2. For the individual tests the standard deviation ranged from 0.02 kJ/m^2 to 3.77kJ/m^2. About half of the values gathered from these tests showed good agreement with those from literature.

Another main objective of this study was determining the degree of confidence in the values generated. Since better agreement was reached for values generated during the mode I tests, it can be concluded that a higher level of confidence is given to these values. Mode II results do not carry the same confidence. The TLD results are significantly more conservative than the individual tests. This could be a result of the TLD samples' reluctance to fracture during testing.

As noted before, the TLD did not perform as well in mode II. While TLD adhesive test groups did show moderate agreement, the confidence in the resulting cohesive values is low due to the testing difficulties. The overall complexity of the TLD and its necessary post processing could be reasons for the discrepancy of the results. For mode II, more confidence is given to the individual tests due to the reduced risk of data manipulation inherent in the simplicity of the test. Overall, the individual tests have less sources for error, and as long as the assumptions used by the tests are deemed correct, the resulting values have the most confidence.

5 Conclusions

To address the need for better analysis methods for adhesives, a study was conducted to collect cohesive properties of four aerospace adhesives and one common place adhesive. Different tests were used to collect these values; a series of simple individual tests and a traction law device. The TLD is able to capture mode I and mode II TLC which can then be used to determine cohesive toughness and strength values. The simple tests are used to gather individual strength and toughness values for both mode I and mode II. Great care was taken to ensure good bonding of the adhesives to the substrate material. Surface preparation methods were used to create a clean, abraded aluminum surface to bond to. Good adhesion was achieved in the majority of the tests conducted. Good agreement was found between values generated from the TLD and from the individual tests for mode I. TLD values for mode II did not have good agreement with individual tests. The simple individual test values carry more confidence due to the nature of the testing and the good agreement between samples. Further development of the TLD could be used to help alleviate discrepancies that arose during this study. In general, if one does not require the true shape of the TLC, the simple tests are the desired testing method for gathering cohesive values. Further investigations into the importance of TLC shape on FE study results could add insight into the use of the TLD. Optimization of the TLD to reduce set up time would also make the device more appealing to use. The values generated by the individual tests are suitable for further study using CZM and should provide reliable cohesive parameters to model the adhesive studied.

6 Bibliography

[1] j. D. Minford, Handbook of aluminum bonding technology and data, New York: MARCEL DEKKER, INC., 1993.

[2] Y. X. Q. Z. P.-C. W. K. W. Xin Yang, "Modeling of high strength steel joints bonded with toughened adhesive for vehicle crash simulations," *International Journal of Adhesion & Adhesives,* vol. 39, p. 21, 2012.

[3] C. Inglis, "Stresses in a plate due to the presence of cracks and sharp corners," in *54th Session of the Institution of Naval Architects*, Cambridge, 1913.

[4] A.A.Griffith, "The Phnomena of Rapture and Flow in Solids," *Royal Society of London,* vol. 221, pp. 163-198, 1921.

[5] T. Anderson, Fracture Mechanics Fundamentals and Applications, Boca Raton, FL: CRC Press, 2005.

[6] G. Irwin, "Analysis of Stresses and Strains Near the End of a Crack Traversing a Plate," *Journal of Applied Mechanics,* pp. 361-364, 1957.

[7] J. G. J. C. R. C. M.F.S.F. De Moura, "Cohesive and continuum mixed-mode damage models applied to the simulation of mechanical behaviour of bonded joints," *International Journal of Adhesion and Adhesive,* no. 28, pp. 419-426, 2008.

[8] T. K. J. Bent F. Sorensen, "Determination of cohesive laws by the J integral approach," *Engineering Fracture Mechanics,* no. 70, pp. 1841-1858, 2003.

[9] C. L. F. D. T. P. T.Ferracin, "On the determination of cohesive zone properties of an adhesive layer from the analysis of the wedge-peel test," *International Journal of Solids and Structures,* no. 40, pp. 2889-2904, 2003.

[10] T. Megson, "Use of Adhesives," in *Aircraft structures for engineeirng students*, Burlington, MA, Elsevier Ltd, 2007, pp. 394-395.

[11] Boeing, "787 Dreamliner," Boeing, 1995-2012. [Online]. Available: http://www.boeing.com/commercial/787family/background.html. [Accessed 5 2012].

[12] Vigin, "Virgin Galactic," Virgin, 2009-2012. [Online]. Available: http://www.virgingalactic.com/. [Accessed 5 2012].

[13] A. K. M. P. W. T. B.R.K Blackman, "Measuring the mode I adhesive fracture energy, Gic, of structural adhesive joints: the results of an international round-robin," *International Journal of Adhesion and Adhesives,* no. 23, pp. 293-305, 2003.

[14] B. F. Sorensen, "Cohesive law and notch sensitivity of adhesive joints," *Acta Materialia,* no. 50, pp. 1053-1061, 2002.

[15] M. T. J.P. Parmigiani, "The roles of toughness and cohesive strenght on crack deflection at interfaces," *Journal of the Mechanics and Physics of Solids,* no. 54, pp. 266-287, 2006.

[16] A. D1002-05, *Apparent Shear Strength of Single Lap Joint Adhesivly Bonded Metal Specimen by Tension Loading,* ASTM International, 2005.

[17] A. D1876-08, *Standard Test Method for Peal Resistance of Adhesives (T-Peel Test),* ASTM International, 2008.

[18] D.S.Dugdale, "Yielding of Steel Sheets Containing Slits," *Journal of Mechanics, Physics, and Solids,* vol. 8, pp. 100-104, 1959.

[19] G.I.Barenblatt, "The Mathmatical Theory of Equilibrium Cracks in Brittle Fracture," Institute of Geology and Development of Combustible Minierals of the U.S.S.R, Moscow, 1962.

[20] M. M. P. P. A. Hillerborg, "Analysis of crack formation and crack growth in concrete by means of fracture mechanics and finite elements," *Cement and Concrete Research,* vol. 6, no. 6, pp. 733-781, 1976.

[21] A. Needleman, "A continuum model for void nucleation by inclusion dbonding," *Applied Mechanics,* vol. 54, pp. 525-531, 1987.

[22] J. H. V. Tvergaard, "The relation between crack growth resistance and fracture process parameters in elastic-plastic solids," *Mechanics and physics of solids,* vol. 40, pp. 1377-1397, 1992.

[23] I. S. A. C. Karl-Heinz Schwalbe, "The SIAM methode for applying cohesive models to the damage behaviour of engineering materials and structures," *GKSS,* no. 1, pp. 1-78, 2009.

[24] A. B. U. S. Stephan Marzi, "On experimental methods to investigate the effect of layer thickness on the fracure behavior of adhesively bonded joints," *International Journal of Adhesion & Adhesives,* vol. 31, pp. 840-850, 2011.

[25] K. J. T. K. J. a. R. C. O. Bent F. Sorensen, "A general mixed mode fracture mechanics test specimen: The DCB-specimen loaded with uneven bending moments," *Riso National Labratory, Roskilde,* vol. 1394, 2004.

[26] W. R. Li VC, "A novel testing technique for post-peak tensile behaviour of cementitous materials," *Fracture toughness and fracture energy-testing methodes for concrete and rocks,* pp. 183-195, 1989.

[27] J. A. M. K. M.D. Thouless, "Determining the toughness of plastically deforming joints," *Journal of Materials Science* , vol. 33, pp. 189-197, 1998.

[28] M. T. S. W. Q.D. Yang, "Numerical simulations of adhesively-bonded beams failing with extensive plastic deformation," *Journal of Mechanics and Physics of Solids*, no. 47, pp. 1337-1353, 1999.

[29] M. T. Q. Y. S. W. M.S. Kafkalidis, "Deformation and Fracture of Adhesive Layers Constrained by Plastically-Deforming Adherends," *Journal of Adhesion Science and Technology,* vol. 14, no. 13, pp. 1593-1607, 2000.

[30] J. R. Rice, "Mathematical analysis in the mechanics of fracture," in *Mathematical Fundamentals*, New York, Academic Press, 1968, pp. 191-311.

[31] L. Y. a. Y.-W. M. Naghdali Choupani, "Mixed-Mode Fracture of Adhesively Bonded Joints," *Structural Integrity and Fracture,* 2004.

[32] B. S. U. S. J.L. Hogberg, "Constitutive behavior of mixed mode Loaded adhesive layer," *ScienceDirect,* vol. 44, pp. 8335-8354, 2007.

[33] J. P. a. M. D. Thouless, "The effects of cohesive strenght and toughness on mixed-mode delamination of beam-like geometries," University of Michigan, Ann Arbor, 2007.

[34] S. Marzi, "Measuring the critcal energy release rate in Mode II of tough, structural adhesive joints using the Tapered end- notch flexture (TENF) test," *The european physical journal,* vol. 206, pp. 35-40, 2012.

[35] J. W. M. T. S. Li, "The effects of shear on delamination in layered materials," *Journal of the mechanics and physics of solids,* vol. 52, pp. 193-214, 2003.

[36] M. T. Q.D. Yang, "Mixed-Mode fracture analyses of plastically-deforming adhesive joints," *Internationl Journal of Fracture,* vol. 110, pp. 175-187, 2001.

[37] M. T. S. W. Q.D. Yang, "Elastic-plastic mode-II fracture of adhesive joints," *International Journal of Solids and Structures,* vol. 38, pp. 3251-3262, 2001.

[38] L. V. S. M. S. Greg N. Nealson, "Application of Improved Free Edge Digital Image Correlation," in *SAMPE-Tech*, Charleston, SC, 2012.

[39] G. P. B. Shen, "Direct Extraction of Cohesive Fracture Properties from Digital Image Correlation: A Hybrid Inverse Technique," *Experimental Mechanics,* vol. 51, pp. 143-163, 2011.

[40] D. Dynamics, "Basics of 3D Digital Image Correlation," Dantec Gynamics GmbH, Ulm, Germany.

[41] A. International, "Standard Guide for Preeration of Aluminum Surfaces for Structrual Adhesives Bonding (Phosphoric Acid Anodizing)," ASTM International, Conshohocken, Pennsylvania, 2010.

[42] M. T. Q. Y. S. W. M.S. Kafkalidis, "Deformation of fracture of adhesive layers constrained by plastically deforming adherends," *Journal of adhesion science and techology,* vol. 14, no. 13, pp. 1593-1607, 2000.

[43] C.-M. C. C. K. L. Victor C. Li, "Experimental determination of the tension-softening relations for cementitious composites," *Cement and Concrete Research,* vol. 17, no. 3, pp. 441-452, 1987.

[44] W. S. P. E. Y. Y.-K. John Tomblin, "Shear stress-strain data for structural adhesives," Federal Aviation Administration, Wichita, KS, 2002.

[45] K. S. A. A. B. Ulf Stigh, "Measurement of cohesive laws and telated problems," in *ASME 2009 International Mechanical Engineering Congress and Exposition,* Lake Buena Vista, Florida, 2009.

[46] H. K. U. Weerts, "Mixed Mode Fracture Characterization of Adhesive joints," in *ICAS 2000 Congress*, Braunschweig, Germany, 2000.

[47] A. B. Ashwatha Nayaka, "Bond-thickness effects in mode-I fracture of adhesive joints," in *International Conference on Aerospace Science and Technology*, Bangalore, India, 2008.

[48] S. P. T. G.-d. R. A. U. M.R. Gude, "Mode-I adhesive fracture energy of carbon fibre composite joints with nanoreinforced epoxy adhesive," *International Journal of Adhesion and Adhesives,* no. 31, pp. 695-703, 2011.

[49] A. Kinloch, Adhesion and adhesives: science and technology, New York: Chapman and Hall, 1987.

[50] P. K. Bent F Sorensen, "Determination of mixed mode cohesive laws," *Engineering Fracture Mechanics,* no. 73, pp. 2642-2661, 2005.

[51] P. C. P. G. R. I. Hirosi Tada, The Stress Analysis of Cracks Book, Pennsylvania, 1973.

[52] T. Diehl, "Using ABAQUS cohesive elements to model peeling of a epoxy-bonded aluminum strip: a benchmark study for inelastic peel arms," DuPont Engineering Technology, Wilmington, DE, 2005.

APPENDICES

A. Appendix: Sample Preparation

A detailed outline for sample substrate preparation is as follows:

- Machine stock bars to specified geometry
- Clean using “Simple Green” industrial solvent
- Wash with cool tap water and dry with 80psi compressed air
- Check for water break (observe a thin film of water over the bonding surface, if the film does not break a properly cleaned surface has been prepared)
- Light abrasion with 120 to 160 grit sand paper or belt sander
- Clean using Isopropanol
- Cross hatch abrasion using 60 grit sandpaper
- Cleaned with Isopropanol
- Apply Teflon crack initiation strip
- Clean with Isopropanol alcohol
- Apply adhesive, and set in curing fixture.

B. Appendix: Testing Procedure

The following is a step by step summary of the testing and analysis procedure used using the TLD

TLD set up:

- Turn on the INSTORN 4505 and log onto the INSTRON controller computer (this will allow the user to move the INSTRON 5500R crosshead if necessary)

- Start the Bluehill INSTRON software (this will be used to measure crosshead displacement and to later run the test displacement)
- Load the lower TLD fixture to the lower cross head of the INSTRON by inserting the TLD male coupler into the INSTORN female mounting coupler
- Insert mounting pin through the INSTRON female mounting coupler and the TLD male coupler
- Tighten the retaining collar on the TLD male coupler (this secures the TLD male coupler against the INSTRON female mounting coupler)
- Mount the upper TLD mounting plate and upper INSTRON female mounting coupler to the upper cross head of the INSTRON
- Load the upper TLD fixture into the upper INSTRON female mounting coupler the same as the lower
- Insert the mounting pin the same as the lower
- Tighten the retaining collar the same as the lower
- Assemble the moment arms, upper pulleys, and the cable for either mode I or Mode II depending on the test being performed.
- Bolt the upper pulleys to the upper TLD fixture in the appropriate orientation for Mode I or Mode II
- Clip the load cells to the lower TLD fixture anchors using carabineers
- Load the Proof load sample into the Lower TLD mounting rails by inserting the retaining pins through the corresponding holes in the mounting rail couplers and Proof load.
- Bolt the coupler retaining plates to the side of the mounting rail couplers
- Bolt the moment arm couplers to the free end of the Proof load
- Bolt the moment arms to the moment arm couplers.
- Hook the free end of the cable onto the hooks on the load cells

LabVIEW set up:

- Connect the cDAC-9178 to the computer using the USB cable
- Plug in the power supply to the DAC and Log on to the computer
- Mount the NI-9237 load cell module into the DAC
- Connect the RJ-50 Screw terminals to the NI-9237 using the Ethernet cable bundle
- Connect the load cell leads to the RJ-50 Screw terminals
- Load up and run the measurement LabVIEW program (the program reads and writes the load cell and strain gage data)

DIC camera set up:

- Mount the Point Gray Grasshopper GRAS-50S5M cameras on the camera stand (keep the lenses covers on)
- Move the camera stand to the marked locaters in front of the INSTRON
- Connect the cameras to the same computer running LabVIEW using the camera cables (the IEEE 1934 9 pin firewire ports for the camera cables are located on the back of the computer)
- Ensure that external light sources such as the sun are minimized by curtaining off any windows
- Ensure that sufficient light is provided by running the FlyCap2 imaging software and viewing the sample image
- If any area of the sample is washed out (reflecting too much light) cover it with a dull material such as masking tape.
- Adjust the camera image by stretching it to fit the viewing window

- In FlyCap2, under the camera controls tab, in the custom video modes menu adjust the image size to full (Left: 0, Top: 0, Width: 2448, Height: 2048, packet size: 9568) and reduce the image package size to half the max value.
- Set the focal length of the lowest value, and using the camera image focus the cameras on the specimen
- Set the focal length back to 8
- In FlyCap2, open the Camera Settings tab lock the shutter speed and gain
- Adjust the gain to bring the cameras into equal light intensity
- Capture an image of the specimen
- Using the ImageJ software look at a pixel intensity histogram for the special on the sample.
- If the pixel intensity if well distributed the cameras are set up, otherwise adjust the camera gain to lower or raise the pixel intensity.

Testing:

- Preload the cables by moving the cross head down
- Using the LabVIEW program observe the load and bring the cable tension to about 90% of the load cell capacity
- Move the cross head back up and remove the proof load
- To remove the Proof load follow the loading procedure in reverse order (take care not to excessively bend the cables)
- Mount in the test specimen by following the same loading procedure as the Proof load except to add the calibration stops on the mounting pins (these stops allow the specimen to be moved a certain amount for DIC calibration)

- Attach the height cord to one of the sample mounting pins (this will keep the sample at the same height as the TLD move down with the cross head)
- Ensure that the specimen in up against the front calibration stop while adjusting the camera settings
- Remove the camera lenses covers and set up the cameras according to the DIC set up procedure
- Move the specimen back in the fixture up against the rear calibration stop
- Using the DIC calibration grid capture at least 25 calibration image at the crack tip (These images include the DIC calibration grid at difference angles and displacements in the space where the specimen speckle patters will be)
- Insert the dongle USB stick into the computer (this contains licensing information for using the DIC software)
- Use the VIC-3D DIC software verify that your calibration images are good(a score of 0.05 or less is considered good)
- If necessary remove bad calibration images or capture new images.
- Move the specimen forward in the fixture up against the front calibration stop.
- Capture sets of about 10 images of the specimen for a set still frame reference, crosshead displacement, and strain reference. (record the crosshead displacement using Bluehill)
- Process these images using VIC-3D to ensure that the DIC displacement and strain measurements are good
- Move the crosshead down until a very light load (about one to four pound) is applied to the load cells (this ensures that the test will start with little slack in the system)
- Set up the Image capture program to record images every 3 seconds
- Set up the labview program to record load data
- Set up the Bluehill program to displace the crosshead at a constant rate

- Start the image capture program, the LabVIEW recording, and Bluehill program at the same time to begin the test
- Allow the test to run until the specimen fractures
- Stop all the running programs
- Save all the recorded data in an appropriate file where they will all be easy to find
- Return the crosshead to the start position to allow removal of the specimen
- Use the VIC-3D software to analyze the captured test images
- Using the VIC-3D extensometer feature measure the crack opening displacement and export the data to a .csv file

C. Appendix: Analysis Matlab Code

The following is the matlab code used to generate the traction laws from load cell and DIC data

```
%solver to calculate the Mode I cohesive stress and toughness using J
integral approach
%using loadcell data and digital image correlation displacement data
clc
clear all
close all
%Importing data
LabVIEWdata=load('Test000_TLD.txt');    %LabVIEW Data S-Beam Loadcells
DICData=xlsread('Test000_TLD_Displacement.csv');   %DIC Data from Vic3D
Analysis
%Using the Extensometer tool across crack tip
%setting up arrays from LabVIEW data
DICExt=xlsread('Test000_Extenseometer.csv');
Ltime=LabVIEWdata(:,1);                     %[sec] Time column of
LabVIEW data
strain_0=LabVIEWdata(:,2);                  %[Dim]
strain_1=LabVIEWdata(:,3);                  %[Dim]
force_2=LabVIEWdata(:,4)*4.44822162 ;       %[N]
force_3=LabVIEWdata(:,5)*4.44822162 ;       %[N]
Force_2=max(force_2); %[N]
Force_3=max(force_3); %[N]
disp('Max Tension 1')
disp(Force_2)
disp('Max Tension 2')
disp(Force_3)

%setting up arrays from DIC data
DICtime=DICData(:,2);     %[sec] Time column of DIC data
%Xdisplacement=abs(DICData(:,25)/1000);  %[m] X-Displacement of Crack
Tip
Xdisplacement=abs(DICExt(:,4)/1000);  %[m] X-Displacement of Crack Tip
```

```
Ydisplacement=abs(DICData(:,26)/1000);  %[m] Y-Displacement of Crack
Tip
MaxXdisp=max(Xdisplacement);

%setting up arrays from INSTRON data
INSTtime=INSTRONData(:,1);
INSText=INSTRONData(:,2);
INSText=INSTRONData(:,3);

%Beam Geometry
b=22.22/1000;    %[m] Beam Width, Average Measurement (within .01mm)
h=22.22/1000;    %[m] Beam Height, Average Measurement (within .01mm)
y=h/2;           %[m] Distance from the Neutral Axis
I=(b*h^3)/12;    %[m^4] Moment of Inertia for a Rectangular Cantilever
Beam

%Beam Properties - (Change E and v for Stock # values)
E=68.9*10^9;       %[Pa] Young's Modulus (Adhered) [Alcoa Datasheet]
v=0.33;            %[Dim] Poisson's Ratio

%calculating moments and stress
Moment_2=(0.14605.*force_2); %[N-m] 0.14605m = approx. 2*Pulley Radius
%plus distance between pulley centers.
Maxmoment_2=max(Moment_2);
Moment_3=(0.14605.*force_3); %[N-m] 0.14605m = approx. 2*Pulley Radius
%plus distance between pulley centers.
Maxmoment_3=max(Moment_3);



figure (1)
%plotting force data vs. time
hold on
plot(Ltime,force_2,'-b')
plot(Ltime,force_3,'-g')
xlabel('Time (sec)')
ylabel('Load (N)')
title('Load vs. Time')
legend('Load Cell 1','Load Cell 2','Location','NorthWest')
hold off
%plotting the difference force data vs. time
loaddiff=abs((force_2-force_3)./((force_2+force_3)./2)).*100;
figure (2)
plot(Ltime,loaddiff,'-g')
xlabel('Time (sec)')
ylabel('Percent difference ')
title('Percent difference between cable load cells vs. time')
axis([0,1200,0,25])

L1=length(Ltime); %the length of LabVIEW data
L2=length(DICtime); %the length of DICtime data
moment_2=(0.14605*force_2); %[N-m]
moment_3=(0.14605*force_3); %[N-m]
%Calculating J-integral
M1=moment_2;        %[N-m] Moment Applied to the Left Arm of the DCB
M2=moment_3;        %[N-m] Moment Applied to the Right Arm of the DCB
```

```
B=b;                %[m] Width of DCB Sample
H=h;        %[m] Height of DCB Sample

Jext=(1-(v^2))*(21*(M1.^2+M2.^2)-6*M1.*M2)/(4*B^2*H^3*E); %[N/m] equal
to [J/m^2]
JEXT=Jext';
L3=length(Jext); %the Length of Jext
%plotting J-integral vs. data time
figure(3)
plot(Ltime,Jext,'-b')
xlabel('Time (sec)')
ylabel('Jext [N/m^2]')
title('Jext vs. Time')
legend('Jext','Location','NorthWest')
%interpolating displacement data to match J-integral data
a=1;
k=0;
while a==1
    k=.001+k;
SS=1/k; %interpolation step size
DICtime2=DICtime(1):SS:DICtime(L2); %interpolation array
XdispI=(interp1(DICtime,Xdisplacement,DICtime2)); %x displacement
interpolated array
YdispI=(interp1(DICtime,Ydisplacement,DICtime2)); %y displacement
interpolated array
LL1=length(XdispI);
if LL1==L3
    break
end
if k>1000
    disp('Number of Data Set Match Iterations Exceeded')
    break
end
end
%plotting displacement vs time
figure(4)
hold on
plot(DICtime2,XdispI,'r')
plot(DICtime2,YdispI,'b')
xlabel('Time (sec)')
ylabel('Displacment [m]')
title('Displacment vs. Time')
legend('X Displacement','Y Displacement','Location','NorthWest')
hold off

%truncating the Jext, Ltime, DICtime2, xdisp, and ydisp arrays for data
%smoothing purposes
step=11;
k=0;
for i=1:step-1:L3
    k=k+1;
    Jcut(k)=JEXT(i);
    Ltimecut(k)=Ltime(i);
    DICtimecut(k)=DICtime2(i);
    Xdispcut(k)=XdispI(i);
    Ydispcut(k)=YdispI(i);
```

```
end
%assigning a new length variable L4 for the truncated arrays
L4=length(Ltimecut);
%smoothing of the Jcut, xdispcut, and ydispcut arrays
Jsmooth=smooth(Jcut);
Xsmooth1=smooth(Xdispcut);
Ysmooth1=smooth(Ydispcut);
%second round of smoothing
Xsmooth2=smooth(Xsmooth1);
Ysmooth2=smooth(Ysmooth1);
%third round or smoothing
Xsmooth=smooth(Xsmooth2);
Ysmooth=smooth(Ysmooth2);

%displaying the smoothed data
%first is Jsmooth vs Ltimecut
figure(5)
plot(Ltimecut,Jsmooth,'-b')
xlabel('Time (sec)')
ylabel('J smooth [N/m^2]')
title('J smooth vs. Time')
legend('J smooth','Location','NorthWest')
%second is Xsmooth and Ysmooth vs DICtimecut
figure(6)
hold on
plot(DICtimecut,Xsmooth,'-r')
plot(DICtimecut,Ysmooth,'-b')
xlabel('Time (sec)')
ylabel('Displacment Smooth [m]')
title('Displacment Smooth vs. Time')
legend('X Displacement','Y Displacement','Location','NorthWest')
hold off

    %for loop to calculate dJ/dxdisp
    %this loop calculates the Jsmooth and Xsmooth center difference
values,
    %as well as associated time and xdisp array
    Y=0; %setting the zero value for a loop counter
    for i=1:L4-1
        %creating first value in the array
        Y=Y+1;%loop counter
     if i==1
         Jdif(Y)=(Jsmooth(i+1)-Jsmooth(i));
         Xdif(Y)=(Xsmooth(i+1)-Xsmooth(i));
         %createing last value in the array
    elseif i==length(L4)
        Jdif(Y)=(Jsmooth(i)-Jsmooth(i-1));
        Xdif(Y)=(Xsmooth(i)-Xsmooth(i-1));
         %creating all the values inbetween
     else
        Jdif(Y)=(Jsmooth(i+1)-Jsmooth(i-1));
        Xdif(Y)=(Xsmooth(i+1)-Xsmooth(i-1));
     end
         %creating an associated Time array
    Timecut(Y)=Ltimecut(i);
         %creating an associated ydisp array
```

```
    XdispII(Y)=(Xsmooth(i));
    end
    %plotting the center difference values for Jdif and Ydif
    figure(7)
    %first Jdif vs time
    plot(Timecut,Jdif,'r')
    xlabel('Time (sec)')
    ylabel('J step difference [N/m^2]')
    title('J step difference vs. Time')
    figure(8)
    %second Ydif vs time
    plot(Timecut,Xdif,'b')
    xlabel('Time (sec)')
    ylabel('X step difference [m]')
    title('X step difference vs. Time')

%for loop for further truncating the center difference values for
%Jdif, Ydif, Ydisp, and time for smoothing purposes
step2=10; %truncations step size
k2=0; %setting zero value for a loop counter
for i=1:step2-1:L4-1
    k2=k2+1;
    Jdifcut(k2)=Jdif(i);
    Xdifcut(k2)=Xdif(i);
    XdispIcut(k2)=XdispII(i);
    TimeIcut(k2)=Timecut(i);
end
%setting new length variable L5
L5=length(Jdifcut);
%smoothing of the main arrays
Jsmooth1=smooth(Jdifcut);
Xsmooth1=smooth(Xdifcut);
%second round of smoothing
Jsmooth2=smooth(Jsmooth1);
Xsmooth2=smooth(Xsmooth1);
%third round of smoothing
Jsmooth3=smooth(Jsmooth2);
Xsmooth3=smooth(Xsmooth2);
%displaying the smoothed data

    figure(9)
    plot(TimeIcut,Jsmooth3,'r')
    xlabel('Time (sec)')
    ylabel('J step difference smooth [N/m^2]')
    title('J step difference smooth vs. Time')
    figure(10)
    plot(TimeIcut,Xsmooth3,'b')
    xlabel('Time (sec)')
    ylabel('X step difference smooth [N/m^2]')
    title('X step difference smooth vs. Time')
%for loop for cutting off calculating TLMII and cutting off TLMII if it
%goes negative
Y=0; %setting zero value for loop counter
    for i=1:L5
        %creating first value in the array
        Y=Y+1; %loop counter
```

```
   TLMI(Y)=Jsmooth3(i)/Xsmooth3(i); %calculating TLMII
   XdispIcut2(Y)=XdispIcut(i); %creating an associated YdispII array
    end
    %new length variable associated with the break off length of TLMII
    L6=length(TLMI);

%plotting the Traction law
figure(11)
plot(XdispIcut2,TLMI,'-*b')
xlabel('X-disp [m]')
ylabel('TLMI [Pa]')
title('TLMI vs. Xdisp')
L6=20;
for i=1:L6
    CCOD(i)=XdispIcut2(i);
    CSTH(i)=TLMI(i);
end
figure(12)
xlswrite('Test000_XdispIcut2',CCOD')
xlswrite('Test000_TLMI',CSTH')
plot(CCOD,CSTH,'-*b')
xlabel('Crack Opening Displacement [m]')
ylabel('Stress [Pa]')
title('Traction Seperation Curve for Test 028')
```

The following is the matlab code used to calculate the traction law cohesive toughness and stress

```
%solver to calculate toughness and strength values for averaged TLC

clc
clear all
close all

Exceldata=xlsread('Mode I Toughness and Strength Database.xlsx');

[m,n]=size(Exceldata);
x=0;

for I=1:5:n
    x=x+1;
 ACOD=Exceldata(:,I);
 ACS=Exceldata(:,I+1);
 LCS=Exceldata(:,I+3);
 UCS=Exceldata(:,I+4);
 maxACS=max(ACS);
 maxLCS=max(LCS);
 maxUCS=max(UCS);

    for i=1:length(ACOD)-1
        ATough(i)=(ACOD(i+1)-ACOD(i))*((ACS(i)+ACS(i+1))/2);
        LTough(i)=(ACOD(i+1)-ACOD(i))*((LCS(i)+LCS(i+1))/2);
        UTough(i)=(ACOD(i+1)-ACOD(i))*((UCS(i)+UCS(i+1))/2);
    end
```

```
        AToughness(x)=sum(ATough);
        LToughness(x)=sum(LTough);
        UToughness(x)=sum(UTough);

    Datamatrix(x,1)=AToughness(x);
    Datamatrix(x,2)=LToughness(x);
    Datamatrix(x,3)=UToughness(x);
    Datamatrix(x,4)=maxACS;
    Datamatrix(x,5)=maxLCS;
    Datamatrix(x,6)=maxUCS;

end
```

D. Appendix: Individual Test Results Plots

The following plots are for the individual test for cohesive toughness and strength

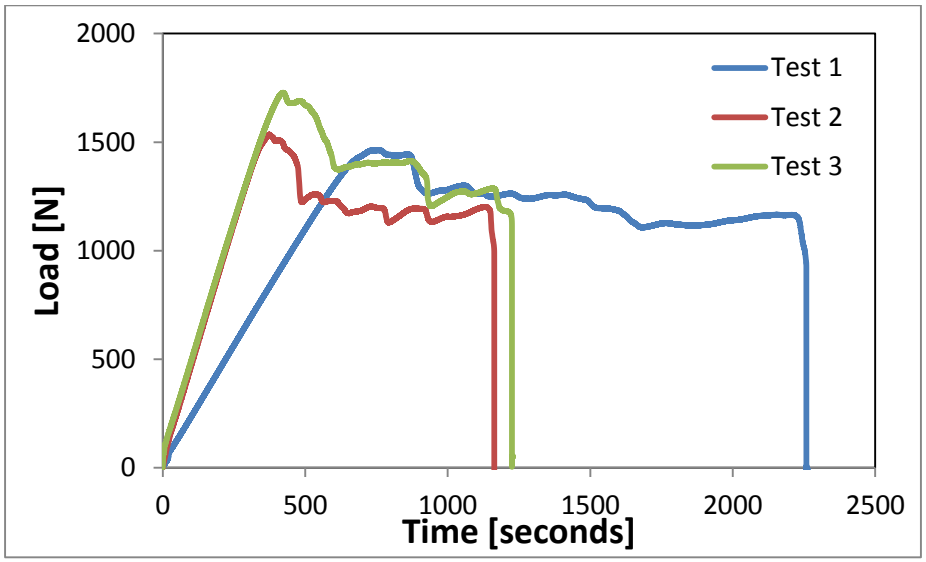

Figure 27: Transversely loaded beam load cell data vs. time for AV4600

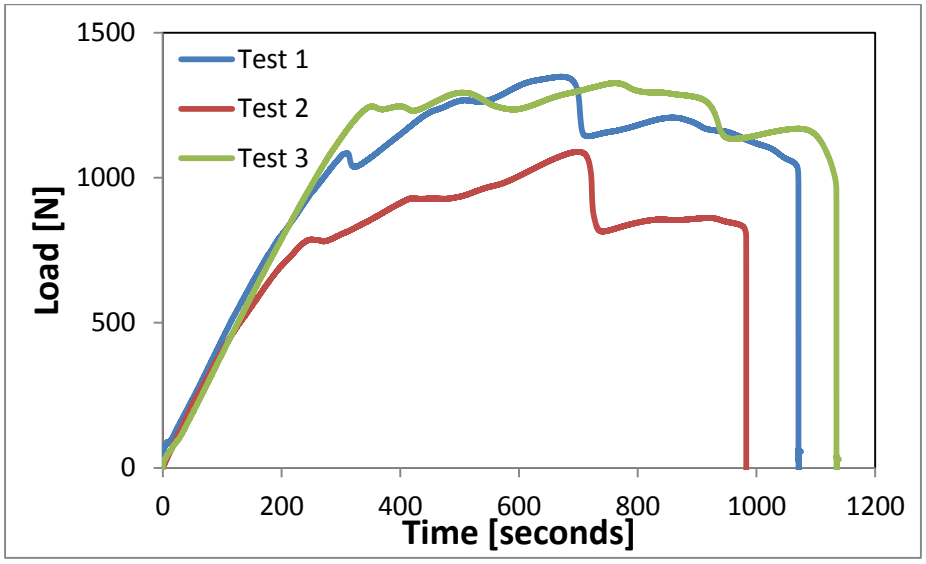

Figure 28: Transversely loaded beam load cell data vs. time for 3M DP 420

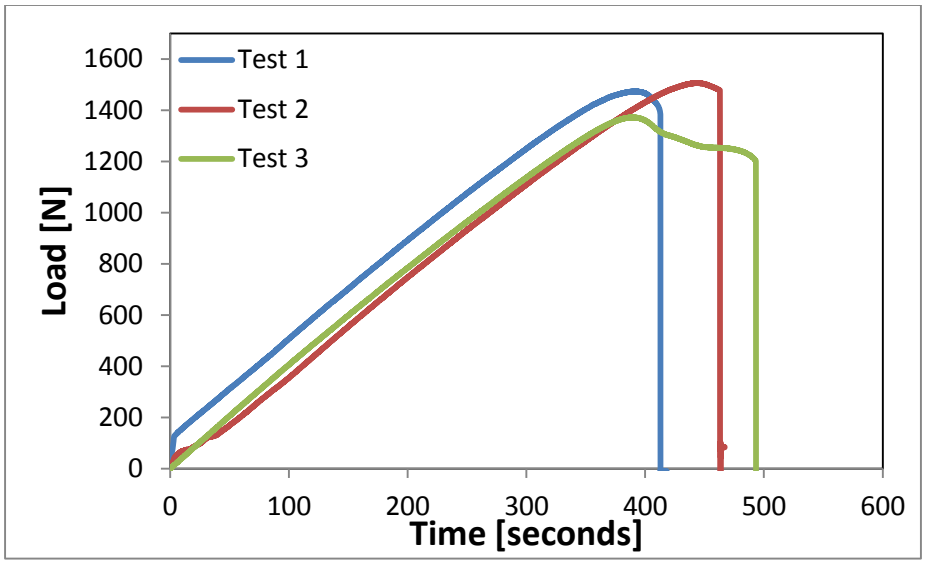

Figure 29: Transversely loaded beam load cell data vs. time for E9539.3

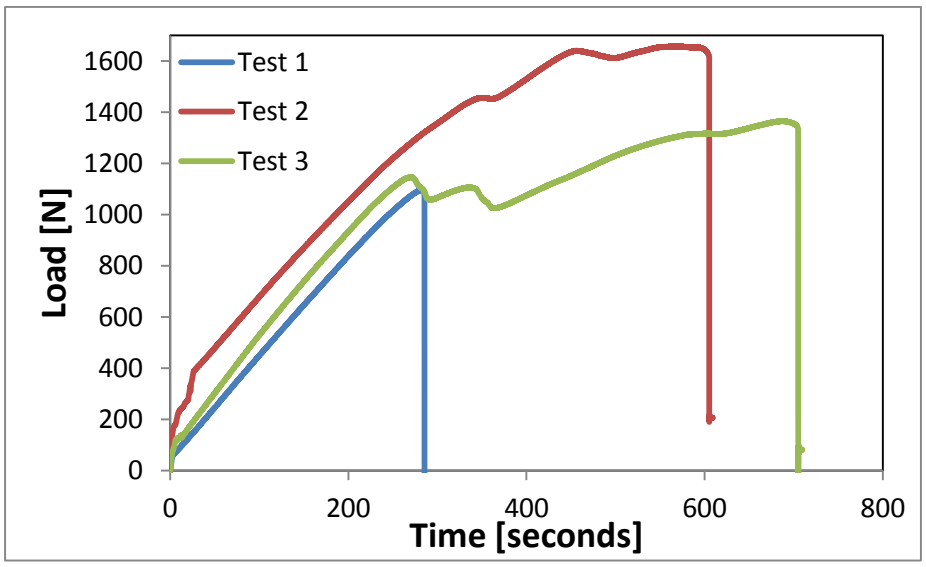

Figure 30: Transversely loaded beam load cell data vs. time for E120

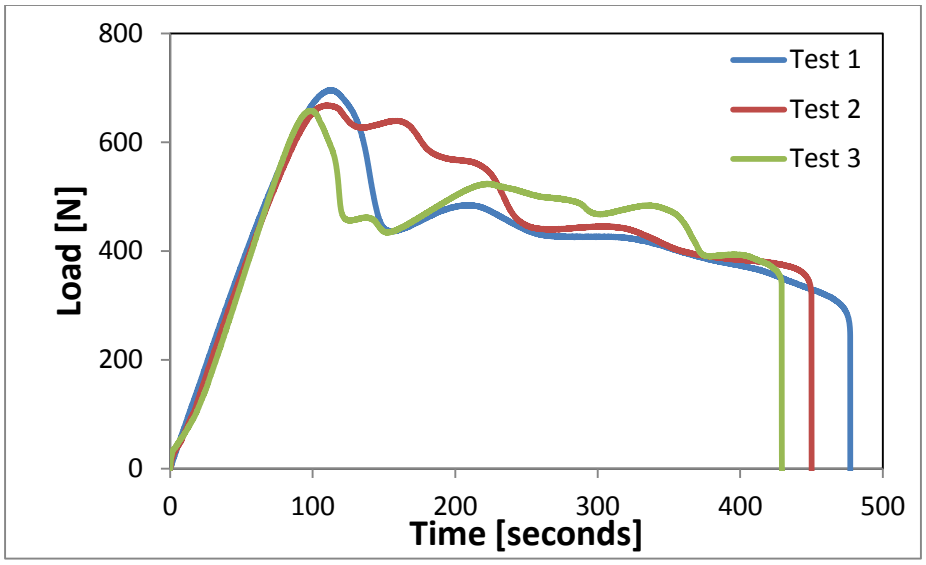

Figure 31: Transversely loaded beam load cell data vs. time for JB Weld

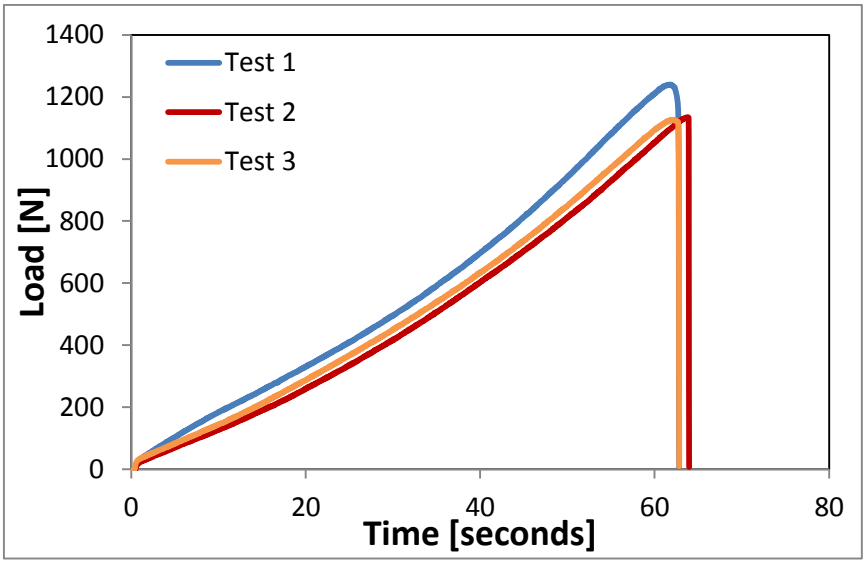

Figure 32: Dogbone ligament load cell data vs. time for AV4600

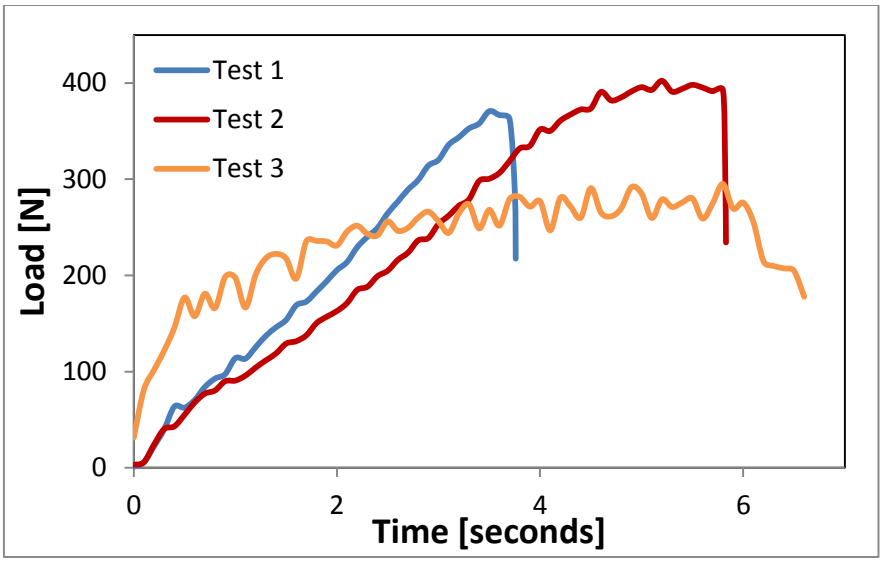

Figure 33: Dogbone ligament load cell data vs. time for 3M DP 420

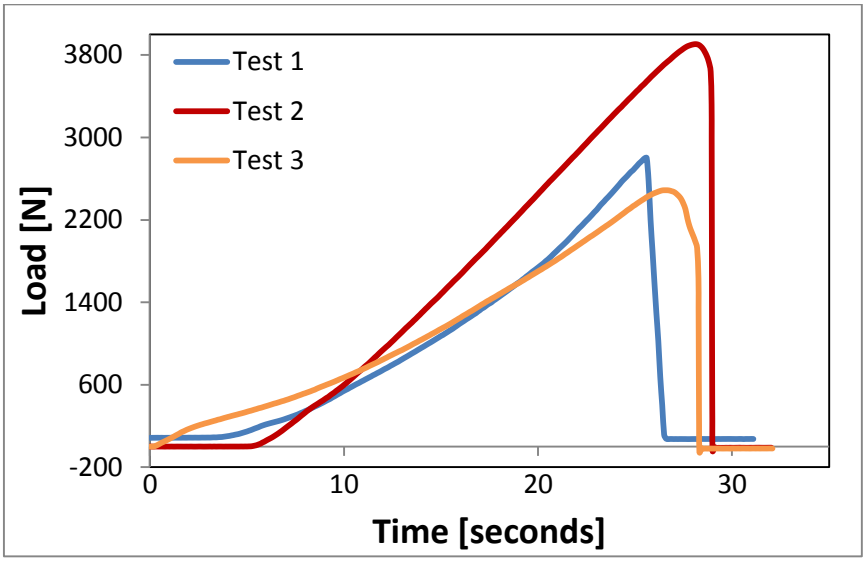

Figure 34: Dogbone ligament load cell data vs. time for E9539.3

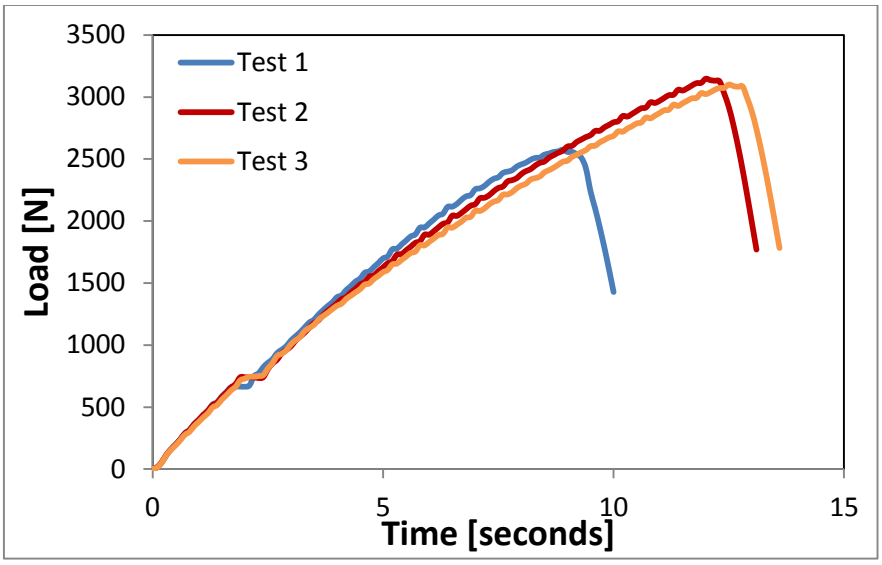

Figure 35: Dogbone Ligament load cell data vs. time for E120

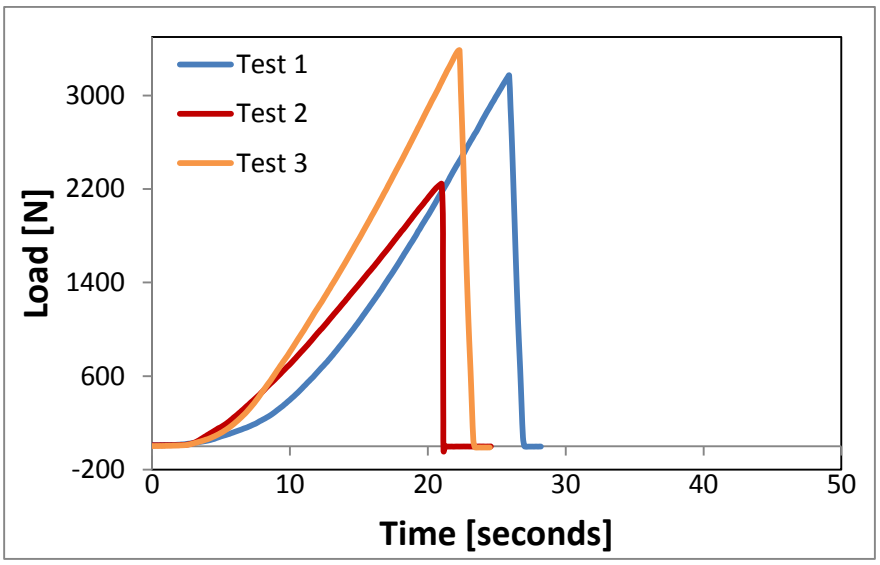

Figure 36: Dogbone ligament load cell data vs. time for JB Weld

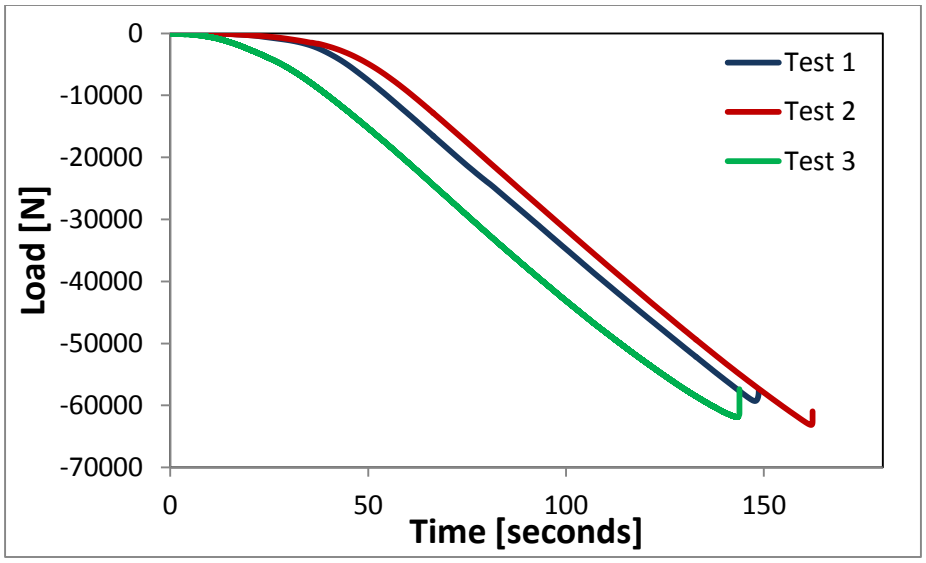

Figure 37: Shear toughness load cell data vs. time for AV4600

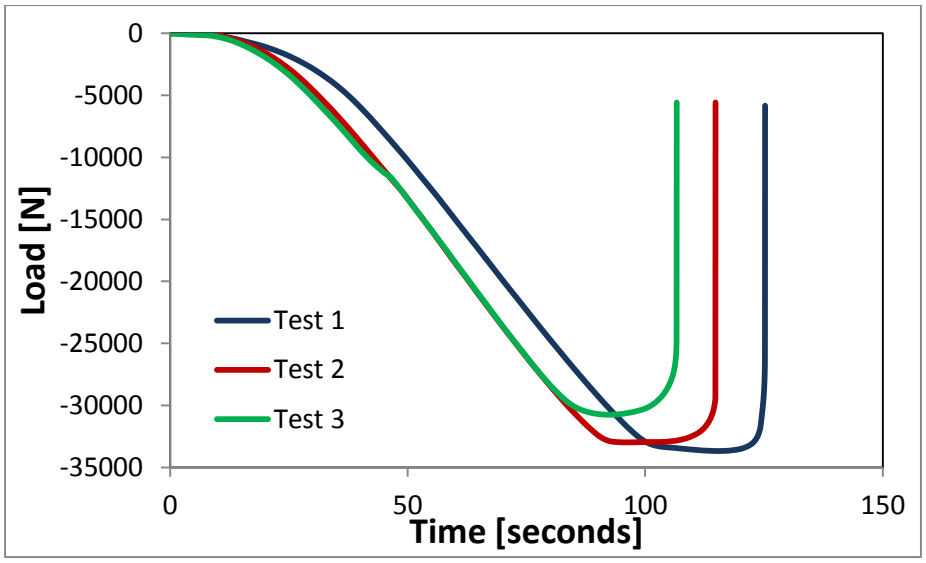

Figure 38: Shear toughness load cell data vs. time for 3M DP 420

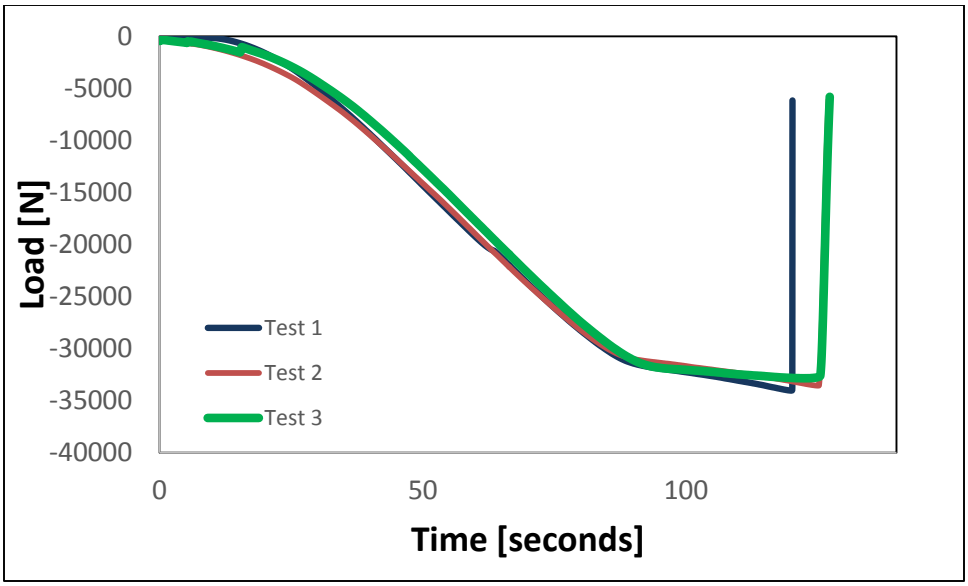

Figure 39: Shear toughness load cell data vs. time for E120

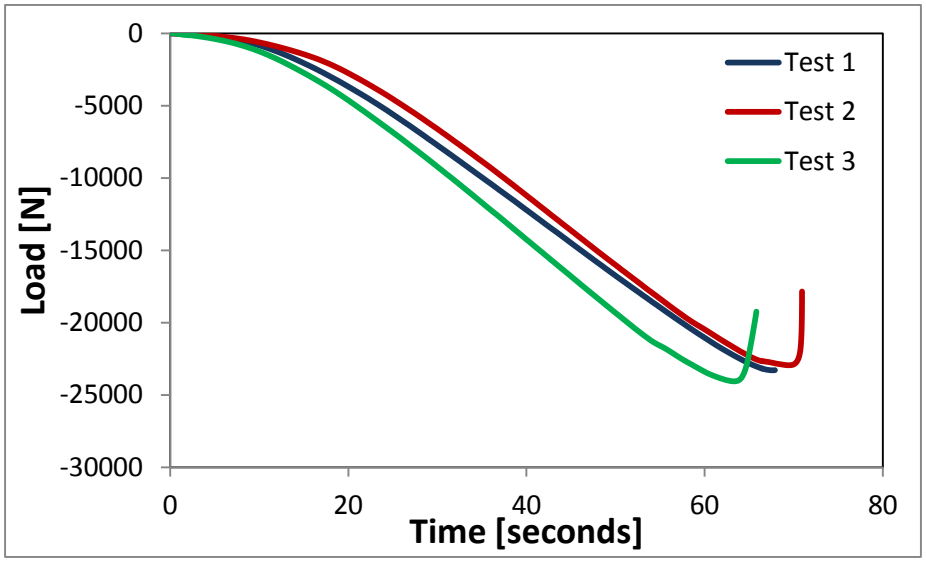

Figure 40: Shear toughness load cell data vs. time for E9539.3

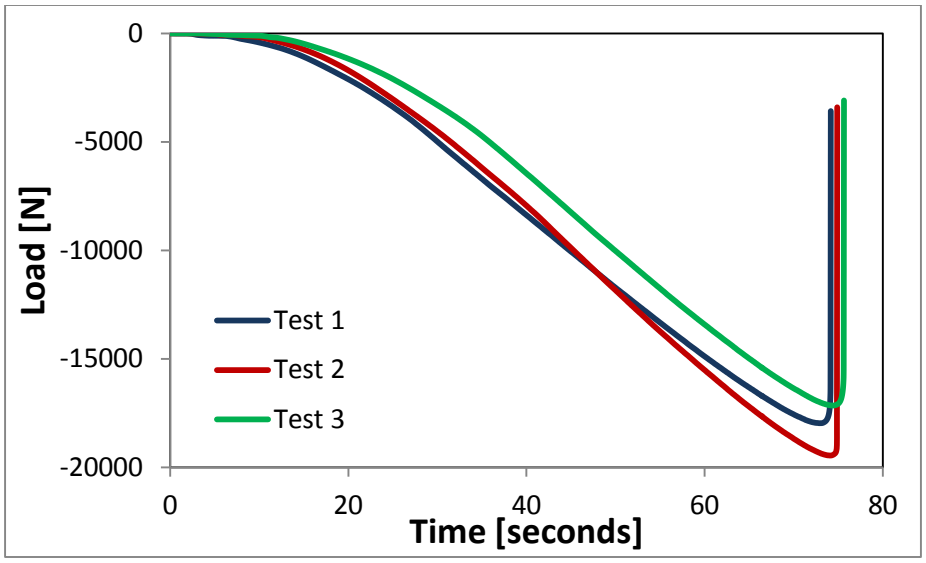

Figure 41: Shear toughness load cell data vs. time for JB Weld

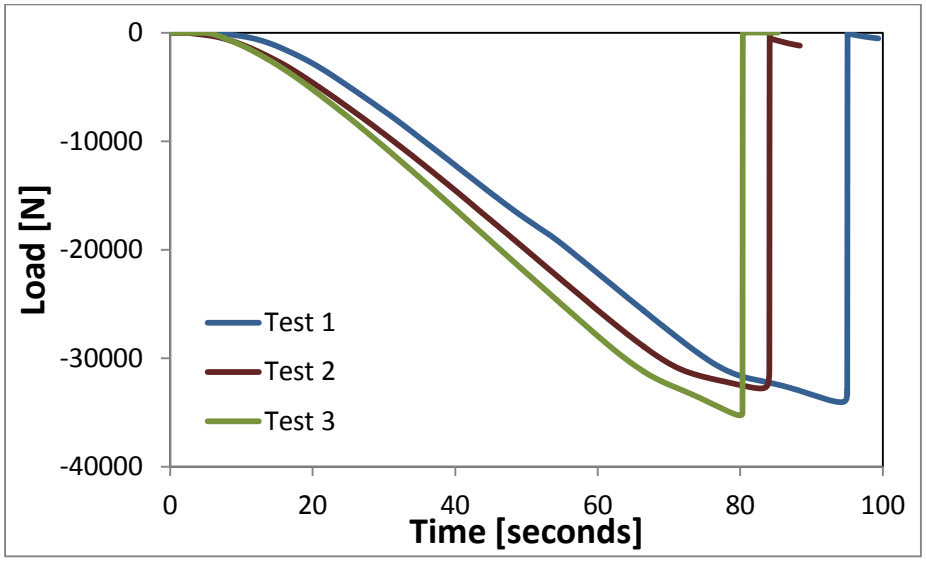

Figure 42: Shear strength load cell data vs. time for AV4600

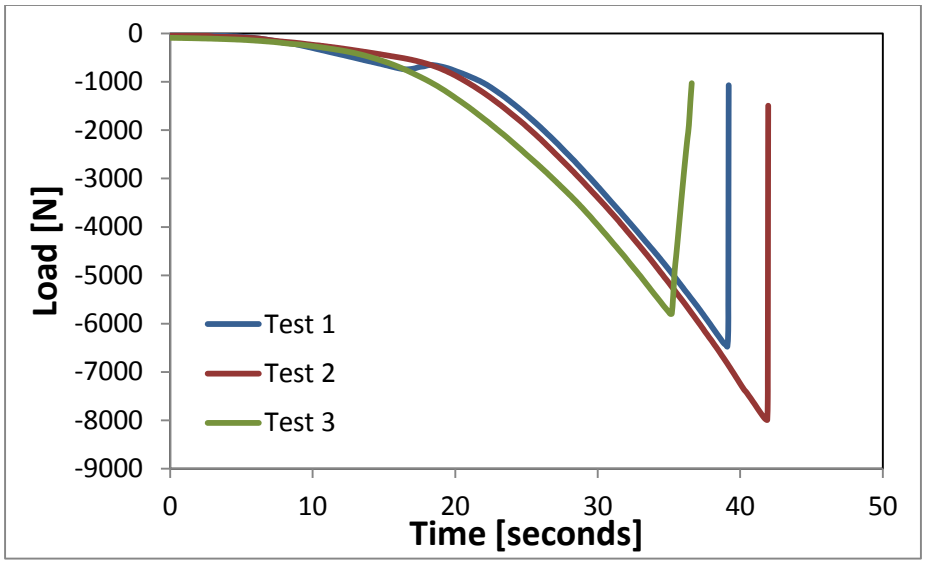

Figure 43: Shear strength load cell data vs. time for 3M DP 420

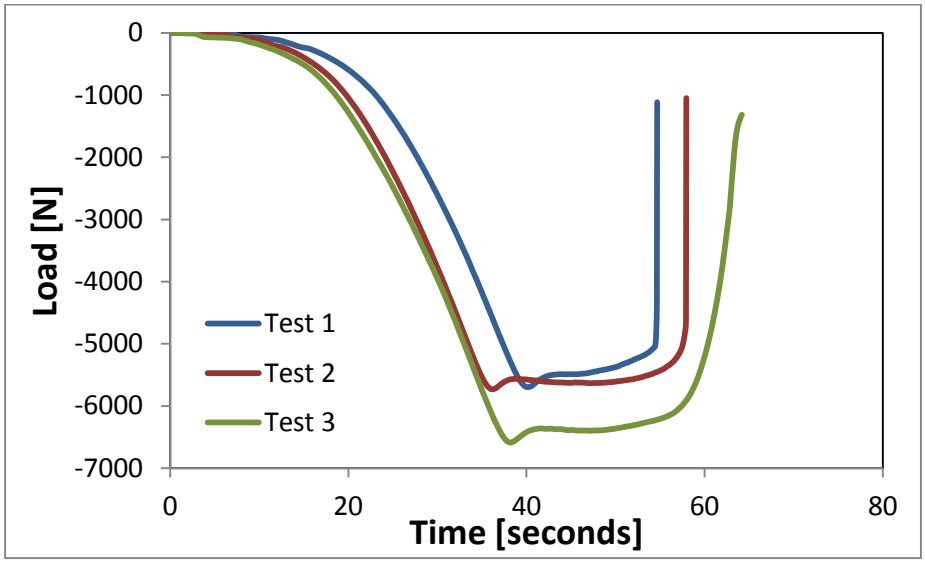

Figure 44: Shear strength load cell data vs. time for E9539.3

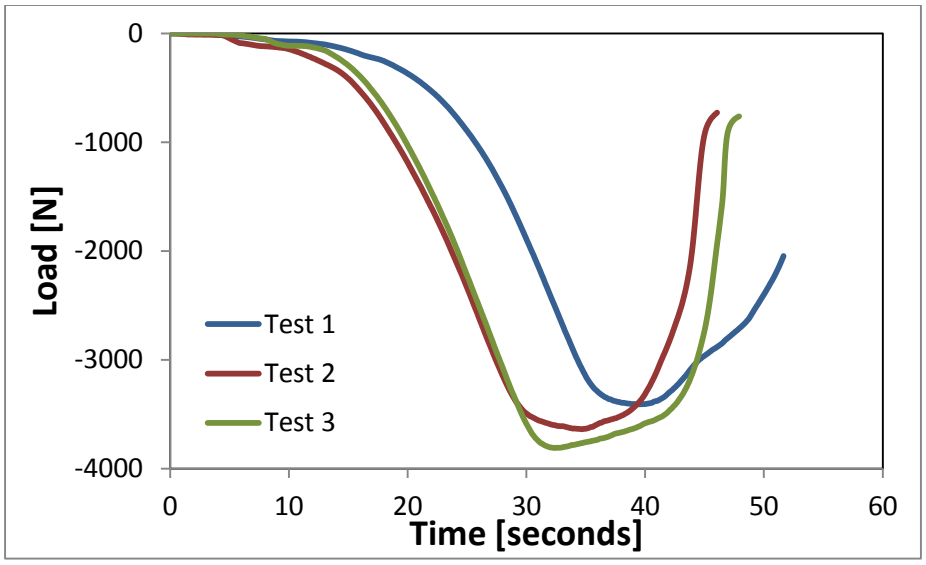

Figure 45: Shear strength load cell data vs. time for E120

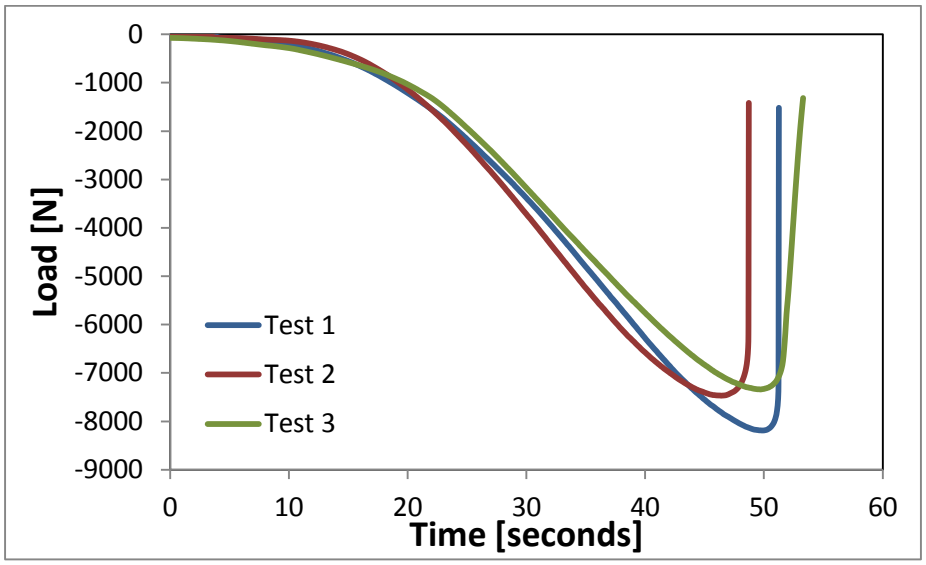

Figure 46: Shear strength load cell data vs. time for JB Weld

E. Appendix: Sample dimension drawings

The following are detailed drawings of the different sample geometries used. All samples drawings are in units of millimeters.

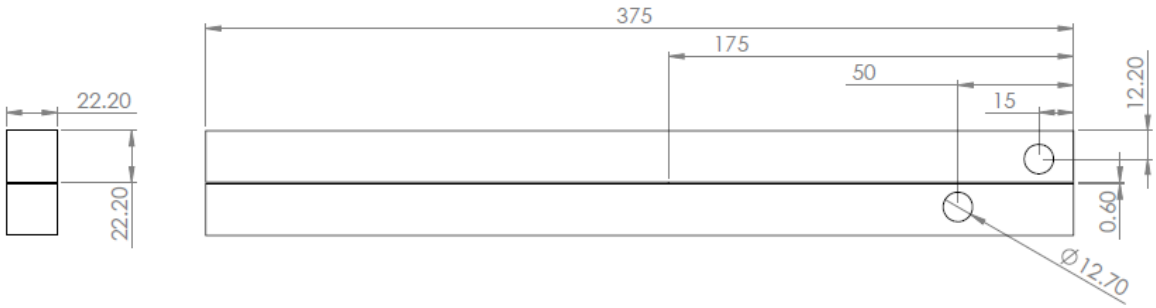

Figure 47: TLD Sample detailed drawing

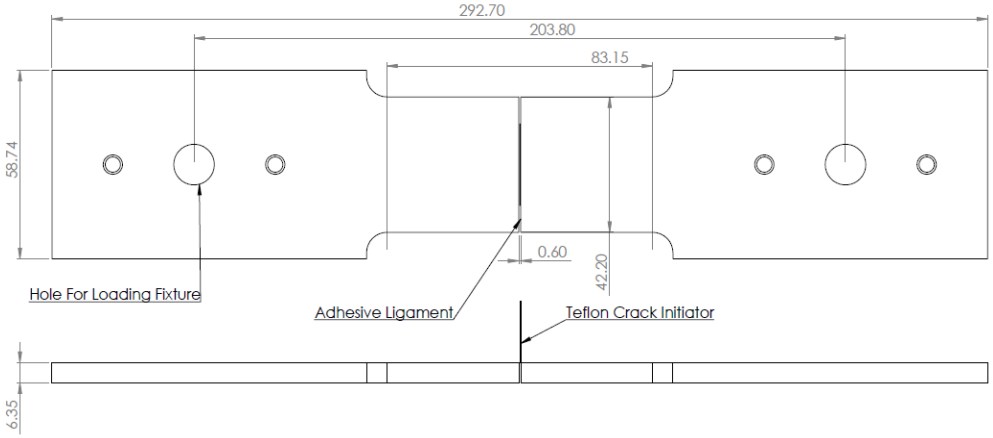

Figure 48: Mode I Dogbone Tension sample detailed drawing

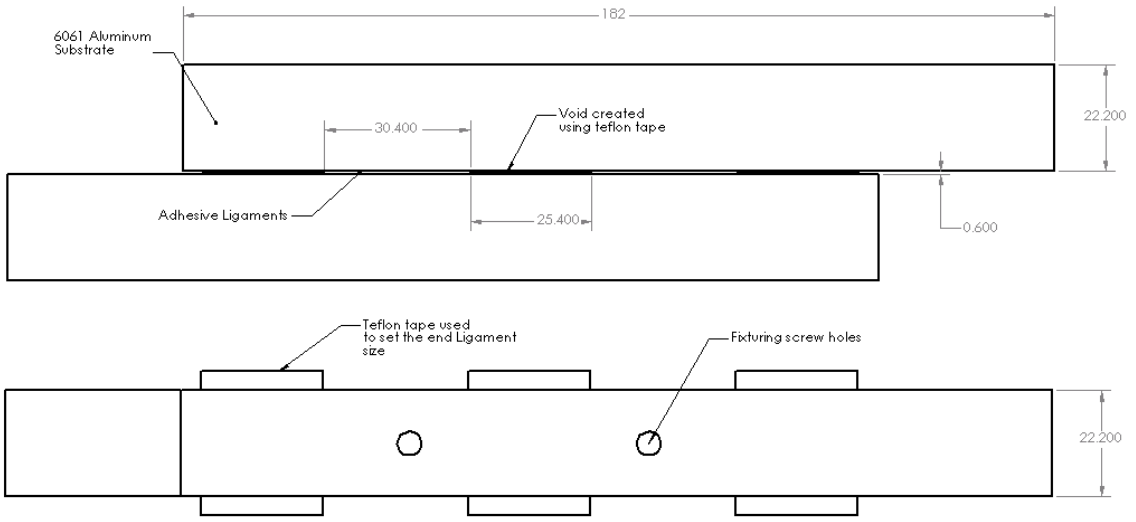

Figure 49: Mode I Shear Ligament sample detailed drawing

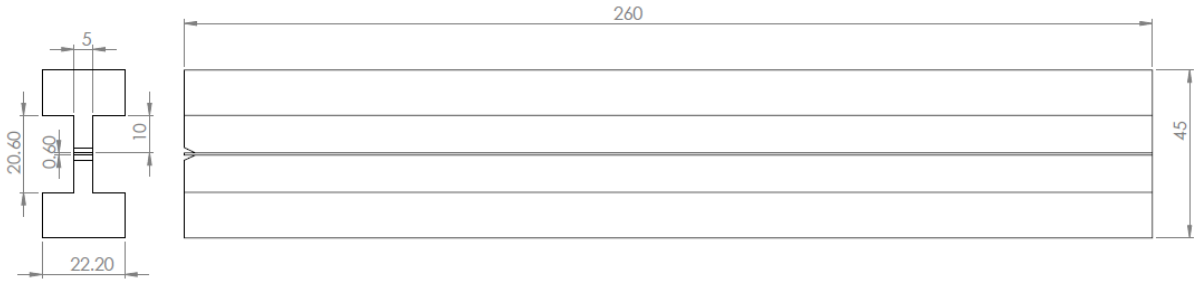

Figure 50: Mode II shear toughness sample detail drawing